Late endosomal transport and tethering are coupled processes controlled by RILP and the cholesterol sensor ORP1L

Rik van der Kant[1], Alexander Fish[2], Lennert Janssen[1], Hans Janssen[1], Sabine Krom[1], Nataschja Ho[1], Thijn Brummelkamp[2], Jan Carette[3], Nuno Rocha[1] and Jacques Neefjes[4,*]

[1]Division of Cell Biology II, The Netherlands Cancer Institute, Plesmanlaan 121, 1066CX Amsterdam, The Netherlands
[2]Division of Biochemistry, The Netherlands Cancer Institute, Plesmanlaan 121, 1066CX Amsterdam, The Netherlands
[3]Department of Microbiology and Immunology, Stanford University School of Medicine, 299 Campus Drive, Stanford, CA 94305, USA
[4]Division of Tumor Biology, The Netherlands Cancer Institute, Plesmanlaan 121, 1066CX Amsterdam, The Netherlands
*Author for correspondence (j.neefjes@nki.nl)

Accepted 2 May 2013
Journal of Cell Science 126, 3462–3474

doi: 10.1242/jcs.129270

Summary

Late endosomes and lysosomes are dynamic organelles that constantly move and fuse to acquire cargo from early endosomes, phagosomes and autophagosome. Defects in lysosomal dynamics cause severe neurodegenerative and developmental diseases, such as Niemann–Pick type C disease and ARC syndrome, yet little is known about the regulation of late endosomal fusion in a mammalian system. Mammalian endosomes destined for fusion need to be transported over very long distances before they tether to initiate contact. Here, we describe that lysosomal tethering and transport are combined processes co-regulated by one multi-protein complex: RAB7–RILP–ORP1L. We show that RILP directly and concomitantly binds the tethering HOPS complex and the $p150^{Glued}$ subunit of the dynein motor. ORP1L then functions as a cholesterol-sensing switch controlling RILP–HOPS–$p150^{Glued}$ interactions. We show that RILP and ORP1L control Ebola virus infection, a process dependent on late endosomal fusion. By combining recruitment and regulation of both the dynein motor and HOPS complex into a single multiprotein complex, the RAB7–RILP–ORP1L complex efficiently couples and regulates the timing of microtubule minus-end transport and fusion, two major events in endosomal biology.

Key words: Endosomal fusion, Ebola virus, HOPS complex, RAB7, RILP, ORP1L, Dynein

Introduction

Intracellular organelles continuously move and fuse due to the activities of motor proteins and fusion complexes. Fusion of organelles occurs in a series of sequential steps starting with transport of organelles along the cytoskeleton towards each other. Subsequently, these organelles tether, dock and fuse to exchange cargo (Bröcker et al., 2010). Early endosomes, autophagosomes and phagosomes fuse with acidic late endosomes and lysosomes (LE) in order to degrade endosomal cargo and recycle nutrients. Defects in the lysosomal transport and fusion machinery result in severe neurodegenerative and developmental diseases such as Niemann–Pick Type C disease (Sobo et al., 2007; Rocha et al., 2009), Charcot–Marie–Tooth disease (CMT) (BasuRay et al., 2013; Spinosa et al., 2008), classical juvenile onset neuronal ceroid lipofuscinosis (Uusi-Rauva et al., 2012) and arthrogryposis, renal dysfunction and cholestasis (ARC) syndrome (Gissen et al., 2004; Cullinane et al., 2010).

Much of our understanding of LE fusion is derived from studies in yeast where vacuolar (lysosomal) tethering is orchestrated by the HOmotypic fusion and vacuole Protein Sorting (HOPS) complex that subsequently interacts with SNARE proteins to induce fusion (Ostrowicz et al., 2010). In contrast to yeast cells, LE in mammalian cells first need to be transported over long distances before they can meet, tether and fuse to exchange cargo. LE transport is well studied in mammalian cells, but tethering for fusion as well as the cross-talk between transport and tethering processes are poorly understood.

In the endo-lysosomal system, various small GTPases of the Rab and Arf family facilitate transport by recruitment of relevant motor proteins from the dynein, kinesin or myosin families (Hoepfner et al., 2005; Wu et al., 2002; Paul et al., 2011; Kuijl et al., 2007; Stenmark, 2009) that specify directionality. The RAB7 effector RILP interacts with the $p150^{Glued}$ subunit of the dynein–dynactin motor complex thus controlling microtubule minus-end transport of late endosomes, lysosomes and lysosome-related organelles such as early melanosomes and cytolytic granules (Johansson et al., 2007; Rocha et al., 2009; Jordens et al., 2001; Daniele et al., 2011; Jordens et al., 2006; Vallee et al., 2012). Silencing of RILP or ectopic expression of its dominant negative N-terminally truncated mutant (RILPΔ199) have been shown to impair endosomal maturation as well as phagosome fusion to lysosomes thereby facilitating intracellular *Salmonella* survival (Marsman et al., 2004; Harrison et al., 2004; Guignot et al., 2004). Dynein motor recruitment to RAB7–RILP is controlled by interactions between the cholesterol sensor ORP1L and the ER protein VAP-A and this mechanism is responsible for vesicle clustering observed in lysosomal storage diseases characterized by accumulation of cholesterol in the late endosomal compartments (Rocha et al., 2009; Vihervaara et al., 2011).

While the spatial control of motor protein recruitment to vesicles is understood at some level of detail, this is not the case for tethering and subsequent fusion of vesicles. Tethering factors function to physically bridge two opposing membranes, establish quality control (i.e. prevent fusion between unrelated compartments) before recruiting SNARE proteins for actual membrane fusion. RAB GTPases are also involved in vesicle tethering and fusion (Bröcker et al., 2010). The RAB5 effector EEA1 can promote docking and fusion of early endosomes (Christoforidis et al., 1999) and other RAB GTPases support multisubunit tethering complexes at the ER, Golgi and the plasma membrane (Bröcker et al., 2010). Late endosomal tethering is best understood in yeast where vacuolar (lysosomal) tethering is orchestrated by the HOPS complex comprising six vacuolar protein-sorting (Vps) components: Vps18, Vps11, Vps16, Vps41, Vps39 and Vps33 (Wickner, 2010). Homologues of all these Vps subunits are found in mammalian systems with some expansion. Specifically two VPS33 proteins exist – VPS33A and VPS33B – and a new VPS33B-interacting protein has evolved: SPE-39 (Huizing et al., 2001; Zhu et al., 2009; Gissen et al., 2005). The yeast RAB7 homologue Ypt7 recruits and assembles the HOPS complex by interacting with Vps39 and Vps41 on different sides of the HOPS complex, suggesting that HOPS bridges Ypt7 on two vesicles (Cabrera et al., 2009; Bröcker et al., 2012).

In yeast, the HOPS complex is the only known Ypt7 effector and no RILP homologue is found. In contrast to mammals, the dynein motor appears to not be essential for late endosomal transport in yeast, indicating that interactions around Ypt7/RAB7 may be different between yeast and human with respect to vesicular transport and tethering functions. Despite significant evolutionary conservation of the actual tethering complex from yeast to human, the current understanding of the HOPS complex composition, recruitment and function in mammalian systems remains limited. Human HOPS has been implicated in EGFR routing (Chirivino et al., 2011) and autophagosome maturation (Liang et al., 2008), and is critical for efficient cytosolic entry of Ebola virus from NPC-1 containing late endosomes (Carette et al., 2011). Mutations in the additional HOPS subunits VPS33b and SPE-39 cause complex multiorgan failures, such as ARC syndrome, which is characterized by impairments in granule secretion and membrane fusion (Gissen et al., 2004; Cullinane et al., 2010). Another HOPS interactor, the small GTPase ARL8b controls lipid loading of CD1 molecules in lysosomes through interactions with some subunits of the HOPS complex (Garg et al., 2011). How the mammalian HOPS complex is recruited to late endosomal membranes, is unclear.

Here, we demonstrate that RAB7 effector RILP recruits the mammalian HOPS complex to late endosomal membranes, and an ARC syndrome disease mutant of VPS33b fails to be recruited to RILP. RILP simultaneously binds both the HOPS complex and dynein motor, thereby coupling transport and tethering for fusion in one protein complex. Uncoupling these processes has major effects on cargo delivery as illustrated for Ebola infectivity. The cholesterol sensor ORP1L controls RILP–HOPS–dynein-motor interactions and times both transport and tethering. Collectively, our observations suggest that two main aspects of late endosomal life – transport and fusion – are integrated and regulated by a single RAB7–RILP–ORP1L protein complex to promote efficient transport and delivery of late endosomal cargo.

Results

RILP induces late endosomal tethering in the absence of functional dynein motor

The RAB7 effector RILP recruits the $p150^{Glued}$ subunit of the dynein–dynactin motor complex to late endosomal membranes to induce microtubule minus-end transport (Cantalupo et al., 2001; Jordens et al., 2001). Expression of RILP in cells induces late endosomal clustering at the microtubule-organizing centre (MTOC) of cells (Rocha et al., 2009; Cantalupo et al., 2001; Jordens et al., 2001) (Fig. 1A) due to dynein motor activity. As active GTP-bound Ypt7 (the yeast RAB7 homologue) is involved in late endosomal tethering (Cabrera et al., 2009) and RILP locks RAB7 in an active GTP-bound state, we wondered whether RILP present on LE might also induce its tethering. To test this, we expressed RILP in cells where dynein motor activity was abrogated by overexpressing $p50^{dynamitin}$ (Fig. 1A) or silencing the dynein chain (DHC) (Fig. 1B). As DHC is 500 kDa and difficult to assess by SDS-PAGE, protein expression was determined by its surrogate marker dynein intermediate chain (DIC) that is stable only in presence of DHC. DIC was efficiently eliminated when DHC was silenced. Under these conditions RILP-labelled endosomes remained in one or two large clusters per cell. These data show that RILP induces LE clustering even in the absence of functional dynein motor, and that RILP might be involved in tethering LEs. To visualize the clusters induced by RILP expression in higher resolution, MelJuSo cells were transfected with GFP–RILP, fixed and sections stained with anti-GFP (10-nm gold) antibodies for analysis by electron microscopy. RILP was often observed at contact sites between LE (Fig. 1C), again suggesting a link between RILP and tethering. LE tethering in yeast is achieved by the HOPS complex which is recruited to LE membranes via the small RAB GTPase Ypt7. To test the localization of the HOPS complex in mammalian cells, we reconstituted a VPS11 knockout (KO) cell line (Carette et al., 2011) with GFP–VPS11. GFP-tagged VPS11 could be successfully incorporated into high molecular mass complexes similar to their endogenous equivalents as assessed by gel filtration and western blotting (Fig. 1D) and a cytosolic distribution was observed for VPS11 (Fig. 1E). To test whether RILP promotes HOPS recruitment to late endosomes, we co-expressed RILP in the GFP–VPS11-expressing cells. In this case, we observed a striking recruitment of VPS11 to RILP-labelled late endosomes (Fig. 1E). While the C-terminus of RILP binds and locks RAB7 in a GTP-bound state, the N-terminus of RILP directly binds the dynein motor (Johansson et al., 2007). Expression of an N-terminally truncated RILP mutant (RILPΔ199) in GFP–VPS11 expressing cells failed to recruit VPS11 to LE (Fig. 1E). These data suggest that the N-terminus of RILP, recruits the dynein motor and is also involved in recruitment of the HOPS complex to late endosomes for tethering.

Mammalian HOPS is recruited to membranes by RILP and regulated by ORP1L

To study localization of the other mammalian HOPS complex subunits, we co-expressed the eight (tagged) HOPS complex subunits in the melanoma cell line MelJuSo (S1A, S1B). Expression levels were moderate (supplementary material Fig. S1C) and the epitope-tagged proteins were successfully incorporated into high molecular mass complexes similar to their endogenous equivalents as determined by gel filtration

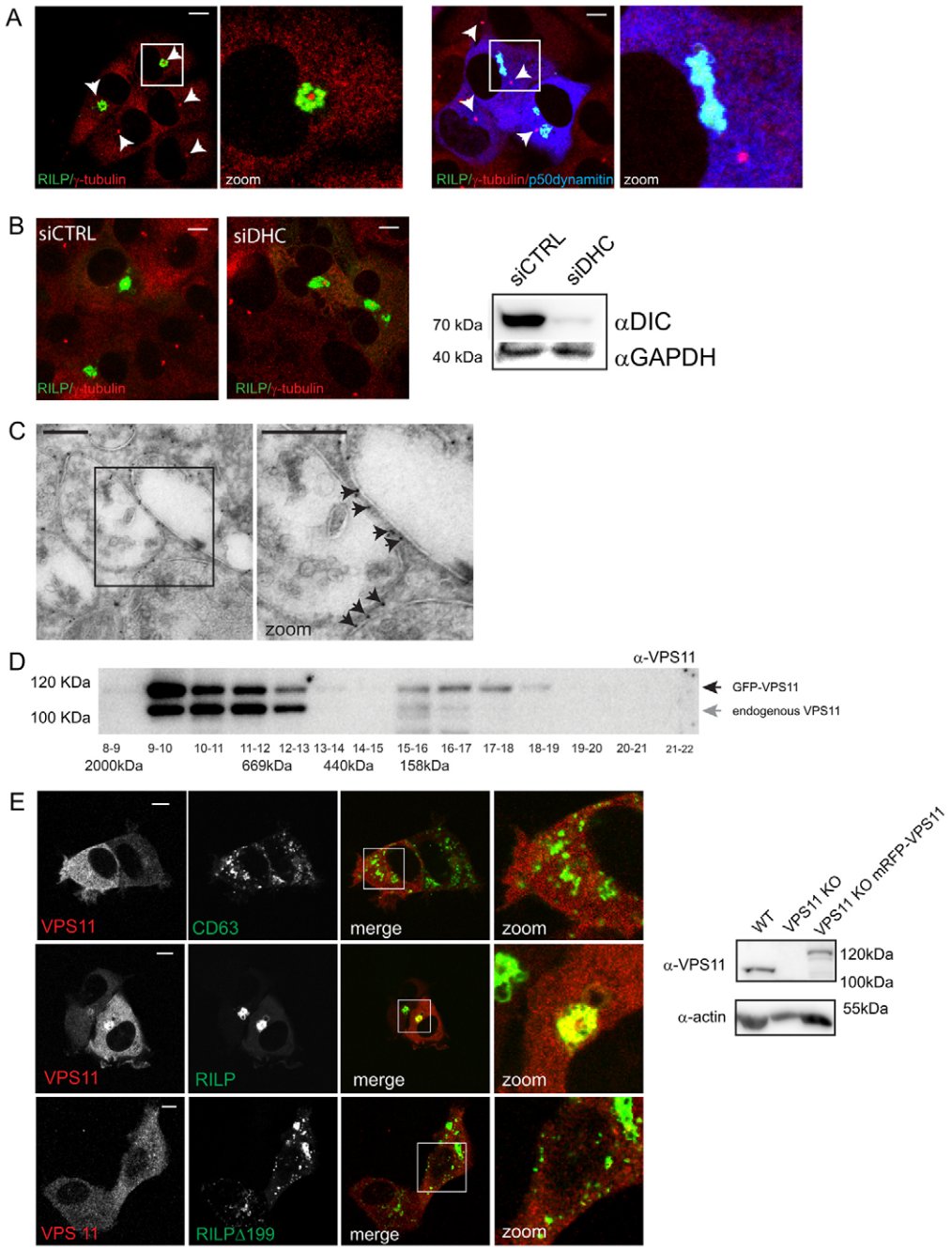

Fig. 1. RILP induces late endosomal tethering independent of dynein-motor recruitment. (**A**) MelJuSo cells expressing HA–RILP and either co-expressing mRFP-p50^{dynamitin} (blue) or not were fixed, immunolabelled with anti-HA (green) and anti-γ-tubulin (red) antibodies and imaged by CLSM. Representative images from $n>100$ are shown. Arrowheads indicate MTOCs. (**B**) Left: MelJuSo cells silenced for dynein heavy chain (DHC) and expressing HA–RILP were fixed, immunolabelled with anti-HA (green) and anti-γ-tubulin (red) antibodies and imaged by CLSM. Representative images from $n>100$ are shown. Right: western blot showing silencing for dynein heavy chain by staining for co-depleted dynein intermediate chain (Raaijmakers et al., 2012). (**C**) Electron micrograph of tethered late endosomal multivesicular bodies in MelJuSo cells expressing GFP–RILP. Sections were stained with anti-GFP antibodies (15-nm gold particles). Right: zoom-in of boxed region in the left overview image. (**D**) Tagged VPS11 is incorporated into high molecular mass complexes. Lysates of MelJuSo cells expressing GFP-tagged VPS11 were size separated by gel filtration. The elution of control proteins (and their mass) is indicated. Fractions of different sizes were separated by SDS-PAGE and western blot, and probed with anti-VPS11 antibody to detect complexes containing GFP-tagged (black arrow) and endogenous VPS11 (gray arrow). (**E**) Left panels: VPS11 KO HAP1 cells expressing mRFP–VPS11 were transfected with GFP–RILP or GFP–RILPΔ199. Merge shows co-localization of VPS11 and RILP. Representative images from $n>100$ are shown. Right panel: expression levels of endogenous and ectopically expressed mRFP–VPS11. Lysates of the WT, VPS11 knockout and the reconstituted HAP1 cells were separated by SDS-PAGE and western blotted with an anti-VPS11 antibody. Actin staining is used as a loading control. Scale bars: 10 µm (A,B,E); 250 nm (C).

(supplementary material Fig. S1D). A cytosolic distribution for all of the HOPS complex subunits was observed upon ectopic expression. Additional expression of constitutively active RAB7 did not suffice to induce recruitment of HOPS to LE (Fig. 2A; supplementary material Fig. S1A,B). However, when co-expressed with RILP (supplementary material Fig. S1A,B) seven of the eight HOPS subunits were recruited to RILP-decorated late endosomes. Only VPS33a was not recruited to RILP unless its interaction partner VPS16 was co-expressed (supplementary material Fig. S1B). Mutations in one of the HOPS complex subunits, VPS33b, causes ARC syndrome and one disease mutant of VPS33b (L30P), has been reported to be deficient in membrane recruitment (Gissen et al., 2004). Indeed, the latter VPS33b mutant failed to be recruited by RILP to late endosomes (Fig. 2B). To further confirm interactions between HOPS and RILP, we performed co-immunoprecipitation experiments. RILP could be co-isolated with VPS11, VPS18 as well as SPE-39 (Fig. 2C).

Binding of the dynein motor to RAB7–RILP is controlled by the cholesterol sensor ORP1L (Rocha et al., 2009). ORP1L also binds RAB7 and prevents binding of the dynein motor to RILP under low cholesterol conditions, as ORP1L then binds to ER protein VAP-A which removes p150^{Glued} from RILP (Rocha et al., 2009). To test if ORP1L also controls RILP-HOPS interactions, we co-expressed various subunits of the HOPS complex with RILP and wild-type ORP1L or a mutant of ORP1L

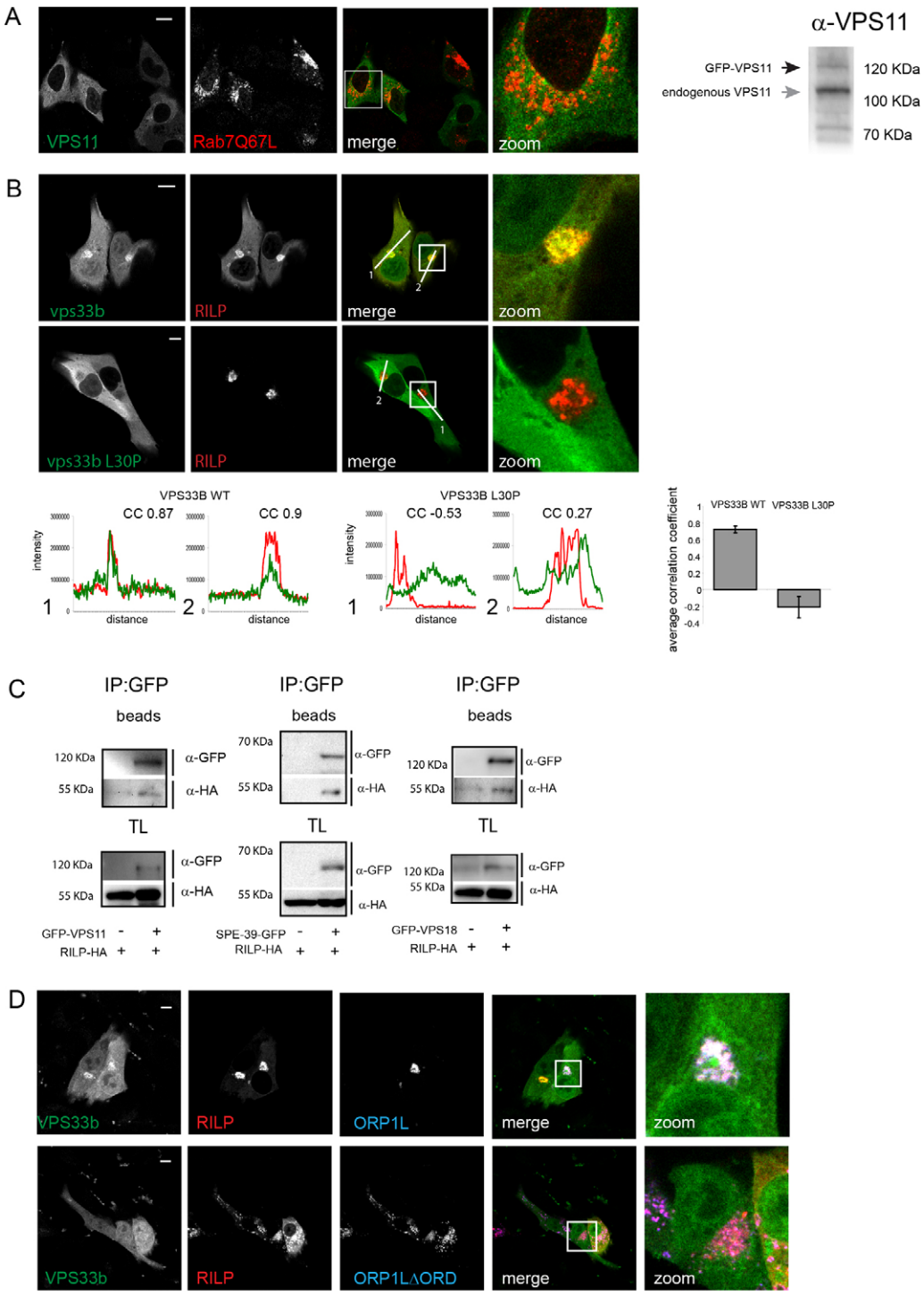

Fig. 2. Mammalian HOPS is recruited to membranes by RILP and regulated by ORP1L. (**A**) Left panels: MelJuSo cells expressing GFP–VPS11 in combination with Myc–RAB7Q67L were stained with anti-Myc antibodies and imaged by confocal microscopy. Zoom images show the boxed area from the merge images. Representative images from $n>100$ are shown. Right panel: expression level of GFP–VPS11 (gray arrow) compared with endogenous VPS11 (black arrow) as assessed by western blotting and probing with anti-VPS11 antibody. (**B**) MelJuSo cells expressing GFP-VPS33b or GFP-VPS33b L30P in combination with RILP-HA were stained with HA-antibodies and imaged by confocal microscopy. Zoom images show the boxed area from the merge images. Representative images from $n>100$ are shown. Plot profiles for cells are shown in lower panels. Red, mRFP intensity; green, GFP intensity (VPS33b) over the sections shown in the indicated in upper panels. Graphs show the average correlation coefficient (CC) + s.e.m. ($n>25$). (**C**) Interaction of SPE39, VPS18 and VPS11 with RILP. Lysates of MelJuSo expressing GFP-tagged HOPS subunits and RILP–HA were immunoprecipitated (IP) with anti-GFP before separation by SDS-PAGE, and western blotting with anti-HA and anti-GFP antibodies. (**D**) MelJuSo cells expressing GFP–VPS33b and RILP–HA in combination with mRFP–ORP1L or mRFP–ORP1LΔORD (as indicated) were immunolabelled with anti-HA antibodies and imaged by confocal microscopy. Zoom images show the boxed area from the merge images. Representative images from $n>100$ are shown. Scale bars: 10 µm.

mimicking low cholesterol conditions (ORP1LΔORD) that releases $p150^{Glued}$ from the RAB7–RILP complex (Fig. 2D; supplementary material Fig. S1E,F). wtORP1L allowed binding of all subunits of the HOPS complex to RILP-labelled endosomes unlike ORP1LΔORD that effectively prevented HOPS subunit recruitment to endosomes (Rocha et al., 2009). Under low cholesterol conditions, ORP1L changes conformation to expose an FFAT motif that subsequently interacts with VAP-A to remove the dynein motor from RAB7–RILP (Rocha et al., 2009). To test whether VAP-A is involved in removing the HOPS complex from RILP under low cholesterol conditions, we repeated the experiments with an ORP1L mutant: ORP1LΔORDFF-AT(D478A) that is similar to ORP1LΔORD with a single mutation in the FFAT domain to abolish interactions with ER protein VAP-A (Rocha et al., 2009) (supplementary material Fig. S1G). This ORP1L mutant again allowed recruitment of HOPS complex subunits to RILP labelled endosomes suggesting that HOPS binding to RILP is – like $p150^{Glued}$ binding – controlled by cholesterol sensor ORP1L through ER protein VAP-A. Together our data indicate that the HOPS complex is recruited to membranes

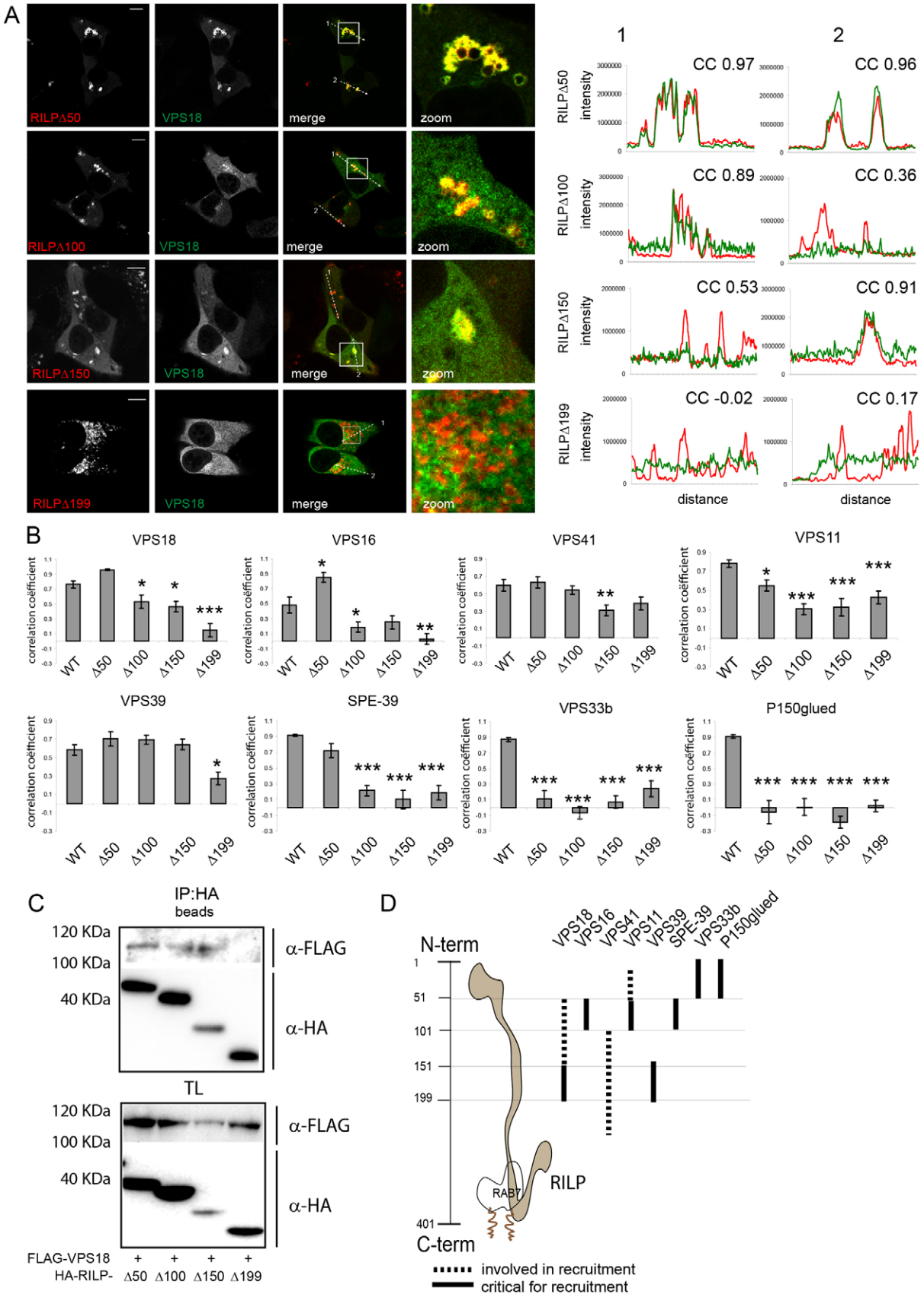

Fig. 3. See next page for legend.

by the RAB7 effector RILP and that recruitment is further regulated by the cholesterol sensor ORP1L.

Fine-mapping of HOPS subunit recruitment to the N-terminus of RILP

In the yeast HOPS complex there are multiple binding sites for Ypt7 (the yeast RAB7 homologue) (Bröcker et al., 2012). To define whether the mammalian HOPS complex interacts with multiple sites on RILP, N-terminal RILP truncations were constructed and expressed with different HOPS complex subunits in MelJuSo cells (Fig. 3A; supplementary material Fig. S2B; quantified in Fig. 3B). Expression levels of the various RILP constructs were similar and all RILP mutants localized properly to late endosomes (supplementary material Fig. S2A). All HOPS subunits [except for VPS33a (supplementary material Fig. S2C)] were recruited to the N-terminal 199 amino acids of RILP that also binds the dynein-motor-complex subunit p150^{Glued} (Johansson et al., 2007). We observed that different HOPS complex subunits were recruited to different regions of RILP (summarized in Fig. 3D). As HOPS subunits were overexpressed, these should be interactions of free HOPS subunits to the different RILP deletion mutants. Recruitment of the entire HOPS complex to RILP probably requires multiple binding sites as deletion of RILP aa 1–100 (disrupting recruitment of VPS11 and VPS16) also negatively affected recruitment of VPS18 (Fig. 3B). These experiments were further confirmed in biochemical experiments where VPS18 was co-isolated with different RILP truncation mutants (Fig. 3C; supplementary material Fig. S2D). While RILPΔ199 failed to co-isolate VPS18, RILPΔ150 and smaller deletion mutants were successful, as also shown in Fig. 3B. Together these data indicate that the mammalian HOPS complex is recruited to late endosomes by multiple interactions with the N-terminal half of the RAB7 effector RILP, the same region that accepts the p150^{Glued} subunit of the dynein motor.

RILP concomitantly binds the dynein motor and HOPS complex

The p150^{Glued} subunit of the dynein motor binds directly to RILP (Johansson et al.). To test if the interactions between RILP and HOPS subunits are also direct, we assayed *in vitro* the binding of two HOPS subunits (VPS18 and VPS41) to RAB7 and/or RILP by SPR. The recombinant proteins used (Fig. 4A) were incorporated into higher molecular mass complexes running at similar complex sizes to endogenous HOPS, indicating that the proteins are well-folded and can interact with their endogenous partners (Fig. 4B). The N-terminus of VPS18 (as for the soluble isolated protein) was shown to be sufficient for recruitment to late endosomes by RILP (supplementary material Fig. S3A) and RAB7/RILP assembled into a stable complex for the SPR experiments (supplementary material Fig. S3B). The recombinant soluble HOPS subunits GST-VPS18 (aa 1–580) and GST–VPS41 were bound to a surface plasmon resonance (SPR) chip and responses were determined in the presence of GTP at different concentrations of RAB7, RILP, the RAB7–RILP complex or the C-terminus of p150^{Glued} (C25) (Fig. 4C). These values were corrected for a GST-only control and from the SPR response curves the equilibrium association constant K_a ($1/K_d$) was determined (Fig. 4C). GTP-loaded RAB7 associated to VPS18 and VPS41 with a low but detectable affinity (4.12×10^4 and 5.80×10^4 M^{-1}, respectively). Binding affinities of RILP to the same HOPS subunits was ~10-fold higher (3.41×10^5 and $5.39\times10^5 M^{-1}$, respectively). The RAB7–RILP complex had a further 2–3 fold increase in affinity for VPS18 and VPS41 (5.98×10^5 and 1.13×10^6 M^{-1}, respectively). No productive binding was detected for VPS18 and VPS41 to C25 ($K_a < 1\times10^4$ M^{-1}). Together our data indicate that both HOPS complex subunits and the C-terminus of p150^{Glued} (Johansson et al., 2007) can associate to RILP in cells and *in vitro*.

This suggests that two general processes in late endosomal life – fusion and transport – are directly coupled through the RAB7-effector RILP. To test this, GFP-tagged VPS41 was co-expressed with RILP and cells were subsequently stained for the dynein motor subunit p150^{Glued}. RILP recruited both p150^{Glued} and VPS41 to clustered endosomes (Fig. 4D). Similar results were obtained with VPS18 (Fig. 4D). To further address whether HOPS and p150^{Glued} bind to RILP simultaneously or mutually exclusive (compete for the same site on RILP), RAB7–RILP and RAB7–RILP–C25 complexes were reconstituted using purified recombinant RAB7, RILP and the C-terminus of p150^{Glued} (C25). Their binding to VPS18 (aa1–580) and VPS41 subunits of the HOPS complex was assessed by SPR (Fig. 4E). Whereas p150^{Glued}–C25 failed to interact with the HOPS subunits, RAB7–RILP–C25 associated with a higher binding affinity than RAB7–RILP only [K_a VPS18 (aa1–580); 1.22×10^6 M^{-1}, VPS41; 1.67×10^6 M^{-1}]. This suggests that the C-terminal part of p150^{Glued} supports, rather than competes for, the interaction of the RAB7–RILP complex to HOPS subunits and that p150^{Glued} and HOPS subunits can simultaneously bind to RILP, effectively integrating a motor protein for transport and a tethering complex for fusion on a single late endosomal receptor: RAB7–RILP.

Late endosomal tethering by RILP and HOPS is required for Ebola virus infectivity

RILP couples late endosomal minus-end transport by the dynein motor complex and tethering by the HOPS complex. Overexpression of RILP induces late endosomal clustering at the MTOC and this clustering is a consequence of p150^{Glued}–dynein-motor recruitment (driving minus-end transport) (Cantalupo et al., 2001; Johansson et al., 2007; Jordens et al., 2001) and HOPS complex recruitment (for vesicle tethering)

Fig. 3. Recruitment of HOPS complex subunits to RILP. (**A**) Left panel: MelJuSo cells expressing GFP–VPS18 and HA-tagged truncation mutants of RILP (Δ50, Δ100, Δ150 and Δ199, respectively) were fixed and stained with anti-HA antibodies before imaging by confocal microscopy. Zoom images show the boxed area from the merge images. Representative images from $n>100$ are shown. Scale bars: 10 µm. Right panel: plot profiles for cells indicated in left panels. Red, mRFP intensity (RILP mutants); Green, GFP intensity (VPS) over the sections shown in left panels. CC, correlation coefficient. (**B**) Quantification of HOPS subunits recruited to RILP mutants. Mean correlation coefficients + s.e.m. are shown for the indicated HOPS subunits. Representative images are shown in supplementary material Fig. S2B. *$P<0.05$, **$P<0.01$ and *** $P<0.001$ when compared with WT RILP; $n>20$ for each condition. (**C**) Interaction of RILP Δ50, Δ100, Δ150 and Δ199 RILP truncation mutants with VPS18. Lysates of MelJuso expressing FLAG-tagged VPS18 and HA–RILP truncation mutants were immunoprecipitated (IP) with anti-HA antibody before separation by SDS-PAGE and western blotting with anti-HA and anti-Flag antibodies. Bottom panel, input; top panel, isolated RILP mutant with co-isolated FLAG–VPS18. (**D**) Map showing the regions of RILP recruiting different HOPS complex subunits and p150^{Glued}, as deduced from Fig. 3B,C and supplementary material Fig. S2B and Fig. S2C.

(Figs 1–4). To study the relative contribution of RILP–HOPS interactions in late endosomal dynamics, we defined RILP mutants that allowed interactions with p150^{Glued} but not with the HOPS complex. To define critical position in RILP to uncouple both processes, we first determined charged amino acids (these are likely exposed to the protein surface) in the N-terminus of RILP and conserved between a series of species. We reversed the charge (for example, R to E or E to R) and tested for recruitment of p150^{Glued} or HOPS subunits (supplementary material Fig. S4A–H). Most mutations that affected RILP interactions with

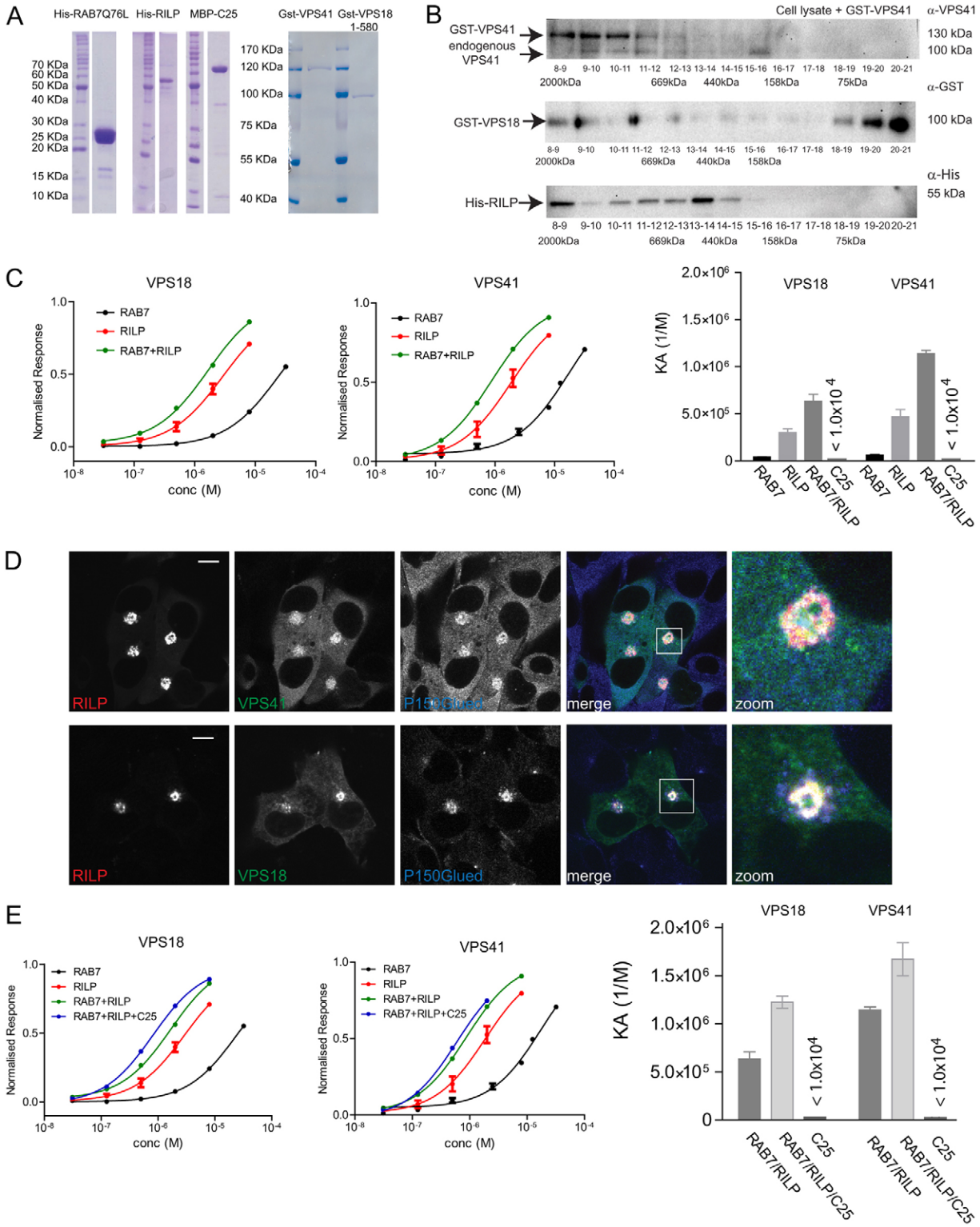

Fig. 4. See next page for legend.

HOPS subunits also affected p150^{Glued} recruitment, suggesting that HOPS stabilizes p150^{Glued} binding to RILP and confirming data from our SPR experiments (Fig. 4). Only one mutant, RILPD125RE126R, markedly affected recruitment of most HOPS subunits with negligible effects on p150^{Glued} recruitment (supplementary material Fig. S4A–H, quantified in Fig. 5A).

To visualize the contribution of HOPS recruitment to late endosomal tethering, we co-expressed RILP mutants and p50^{dynamitin} [to disrupt the dynein motor (Vallee et al., 2012)]. Under these conditions wild-type RILP is still capable of clustering vesicles (Fig. 1). Expression of RILP mutants that fail to recruit the HOPS complex – RILPD125RE126R and RILP E93RE94R – are less potent in clustering LE and in combination with p50^{dynamitin} overexpression yielded cells with many small clusters and single endosomes (Fig. 5B). The experiment was repeated by silencing the DHC subunit of the dynein motor (supplementary material Fig. S4I). Again, RILP mutants unable to recruit HOPS yielded cells with mainly small RILP mutant containing vesicular clusters, indicating that recruitment of HOPS by RILP is required for late endosomal tethering.

A recent genetic screen identified 6 subunits of the HOPS complex as essential for successful cellular infection by Ebola virus (Carette et al., 2011). If RILP is the receptor for the HOPS complex, RILP mutants that fail to recruit the HOPS complex should also affect Ebola virus infection of cells. Cells expressing mRFP, mRFP–RILP, mRFP–RILPΔ199 or mRFP–RILPD125RE126R were infected with replication-competent Vesicular Stomatitis Virus bearing the Ebola virus glycoprotein (rVSV-GP-EboV) (Wong et al., 2010) that produces GFP upon replication in the cytosol of infected cells. rVSV-GP-EboV infectivity was reduced by half in cells expressing mRFP-RILP(D125RE126R) relative to control cells expressing either mRFP only or mRFP-tagged wild-type RILP when infection was assessed by microscopy (Fig. 5C,D) or flow cytometry (supplementary material Fig. S4J). When late endosomal recruitment of both p150^{Glued} and HOPS was prevented with RILPΔ199, inhibition of infection of rVSV-GP-EboV remained attenuated to a level similar as inhibition of HOPS recruitment alone.

As the cholesterol sensor ORP1L acts as regulator of HOPS as well as dynein motor binding to RILP (Rocha et al., 2009) (Fig. 2D), we tested whether ORP1L also affected Ebola virus infection. Cells were transfected with mRFP, mRFP–ORP1L or mRFP–ORP1LΔORD (this mutant abolish RILP–HOPS and RILP–p150^{Glued} interactions) before infection with rVSV-GP-EboV (Fig. 5E). A 50% reduction in rVSV-GP-EboV infectivity in cells expressing mRFP–ORP1LΔORD relative to control cells expressing either mRFP only or mRFP-tagged wild-type ORP1L was observed (Fig. 5E). Collectively, our data suggest that RAB7–RILP is the late endosomal receptor for the HOPS complex and p150^{Glued} and that binding of these complexes to RILP is timed by the cholesterol sensor ORP1L to regulate endosomal maturation.

Fig. 4. Simultaneous binding of HOPS subunits and p150^{Glued} to RILP. (**A**) Coomassie-stained SDS-PAGE gels with the indicated recombinant proteins used for the SPR experiments. The position of marker proteins is shown. (**B**) The recombinant proteins used in SPR studies are incorporated into higher molecular mass complexes. Recombinant GST–VPS41, GST–VPS18(1–512) or His–RILP were incubated with lysates of MelJuSo cells and lysates were subsequently size separated using gel filtration. Fractions were subjected to SDS-PAGE and western blotting with the indicated antibodies to detect complexes containing the recombinant proteins. (**C**) GST–VPS18 (aa 1–580) or GST–VPS41 was immobilized to an SPR chip, and binding of RAB7Q76L, RILP, a RAB7Q76L–RILP complex and C25 in the presence of GTP-γS was determined. RAB7Q76L and RILP were pre-incubated with GTP-γS to assemble the complex. The left panels show the responses (corrected to that of GST only) at different concentrations of RAB7, RILP or the RAB7–RILP complex. Right panel: K_a (mean+s.e.m.) calculated from the SPR responses. Shown is K_a of RAB7Q76L, RILP or RAB7Q76L-RILP binding *in vitro* to VPS18 (aa 1–580) or VPS41, all measured in the presence of GTP-γS. (**D**) MelJuSo cells expressing HA–RILP and GFP–VPS18 or GFP–VPS41 (as indicated) were fixed, immunolabelled with anti-p150^{Glued} and anti-HA antibodies and imaged by CLSM. The zoom images are the boxed area from the merge images and illustrate co-localization of RILP with p150^{Glued} and VPS18 or VPS41. Scale bars: 10 µm. Representative images from $n>100$ are shown. (**E**) Left panels: *in vitro* binding of GST–VPS18 (aa 1–580) or GST–VPS41 immobilized on a SPR chip to RAB7Q76L, RILP, the RAB7Q76L–RILP complex or the RAB7–RILP–C25 (the C-terminal domain of p150^{Glued}) complex (mean+s.e.m.). Binding was determined in the presence of GTP-γS and corrected for binding to GST only coupled to the SPR chip. Right panel: K_a calculated From the SPR responses shown in B. Shown is *in vitro* binding of the C-terminal p150^{Glued} fragment C25, the preformed complex of RAB7Q76L–RILP and RAB7Q67L–RILP–C25 to VPS18 (aa 1–580) and VPS41, all measured in the presence of GTP-γS (means+s.e.m.).

Discussion

The life of a vesicle can be described in a few general terms, including membrane transport and fusion. The small GTP-binding proteins of the Rab/Ypt family have been defined as key regulators of these processes (Stenmark, 2009). One member, RAB7 acts as the late endosome receptor for the dynein motor via its effector RILP (Jordens et al., 2001). In yeast, the RAB7 homologue Ypt7 recruits the HOPS complex to membranes to control correct interaction of late endosomes with vacuoles prior to fusion (Bröcker et al., 2010). Homologues for all yeast HOPS subunits have been found in eukaryotic genomes, and two additional homologues VPS33b and SPE-39 (VPS16B/VIPAR) exist. Deletion or mutations of HOPS subunits *deep orange* (VPS18 homologue), *carnation* (VPS33a homologue) or *dvps16A* (VPS16 homologue) result in defective late endosomal and lysosomal biogenesis in *Drosophila melanogaster* (Pulipparacharuvil et al., 2005; Sevrioukov et al., 1999). Mutations in VPS41 can protect against α-synuclein-induced neurotoxicity in *C. elegans* and Parkinson's disease in mammalian model systems (Harrington et al., 2012; Ruan et al., 2010), and VPS41-deficient mouse embryos fail to develop beyond the gastrulation stage (Aoyama et al., 2012). In addition, the HOPS complex has been implicated in Ebola virus infection, EGFR trafficking, autophagolysosome formation and endosomal peptide loading of CD1d (Carette et al., 2011; Ganley et al., 2011; Chirivino et al., 2011; Garg et al., 2011). Mutations in the additional HOPS subunits VPS33b and SPE-39 cause complex multiorgan failures such as ARC syndrome, which is characterized by impairments in granule secretion and membrane fusion (Gissen et al., 2004; Cullinane et al., 2010). Although the HOPS complex is involved in all these processes, how the HOPS complex is regulated and recruited to late endosomal membranes in mammalian cells remains unclear.

Here we report that in mammals HOPS subunits are not recruited by RAB7 but by the RAB7 effector RILP. Using surface plasmon resonance (SPR) experiments, we demonstrate that HOPS subunits (VPS18 and VPS41) exhibit low affinity for RAB7 alone, 10–15-fold higher affinity for RILP and even higher affinity for RILP associated to RAB7. In evolution, HOPS

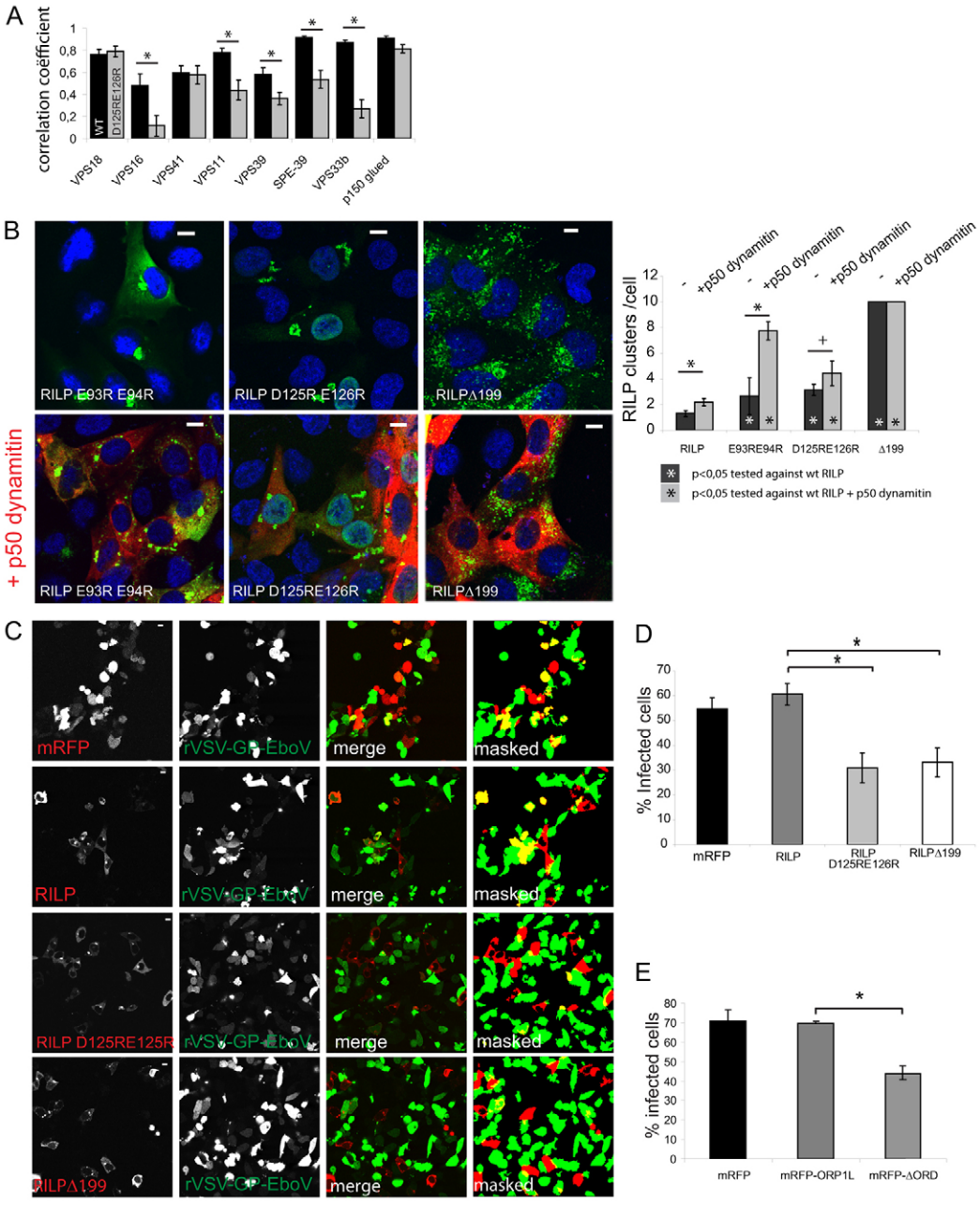

Fig. 5. RILP induces late endosomal tethering. (**A**) Quantification of HOPS subunit recruitment to wild-type RILP (WT, black) and RILP D125RE125R (gray). Mean correlation coefficients (+s.e.m.) are shown for indicated HOPS subunits. *$P<0.05$. $n>20$ for each condition. (**B**) MelJuSo cells expressing HA–RILP, HA–RILPE93RE94R, HARILPD125RE126R and either co-expressing mRFP-p50^{dynamitin} or not were fixed, immunolabelled with anti-HA antibodies (green) and DAPI (blue) and imaged by CLSM. Representative images from $n>100$ are shown. The quantification on the right shows the average number of individual clusters and/or vesicles per cell (means + s.d.). Cells with >10 clusters were set at 10. *$P<0.05$, $^{+}P<0.1$ (**C**) HAP-1 cells expressing mRFP, mRFP–RILP, mRFP–RILPΔ199 or mRFP–RILPD125RE126R were infected with rVSV-GP-EboV for 8 hours. The virus produces GFP in the host cytosol after successful infection, which is detected and quantified. Right panel: cells were identified, masked and overlayed using Cell Profiler. Red, transfected cells; green, cells with successful infection of rVSV-GP-EboV; yellow, transfected and infected cells expressing the mRFP-labelled constructs. (**D**) Quantification of mRFP, mRFP-RILP-, mRFP-RILPΔ199- or mRFP-RILPD125RE126R-expressing cells successfully infected by rVSV-GP-EboV as measured by cytosolic GFP expression (means+s.e.m.). *$P<0.05$. (**E**) HAP-1 cells expressing mRFP, mRFP-ORP1L or mRFP-ORP1L ΔORD were infected with rVSV-GP-EboV for 8 hours. After successful infection, the virus produces GFP in the cytosol which is detected and quantified by flow cytometry. Shown is the percentage of transfected (mRFP-positive) and infected (GFP-positive) cells relative to transfected cells (mean+s.e.m). *$P<0.05$. Scale bars: 10 µm.

recruitment has apparently shifted from RAB7/YPT7 to its effector RILP. RILP also binds the p150^{Glued} subunit of the dynein motor for minus-end-directed microtubule transport (Jordens et al., 2001; Cantalupo et al., 2001). We have mapped recruitment of HOPS to the N-terminus RILP and revealed that there are multiple positions in RILP required for HOPS

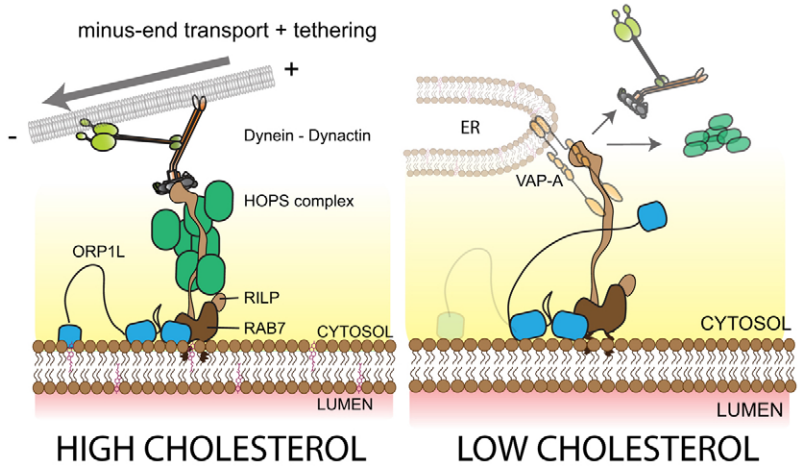

Fig. 6. Model of ORP1L in control of binding of the HOPS complex and dynein–dynactin motor to RAB7–RILP. Late endosomes destined for fusion require close proximity (by minus-end transport) and tethering (by HOPS) for subsequent SNARE-dependent fusion. In high-cholesterol conditions (left panel), ORP1L the dynein motor and the HOPS complex can both bind to RILP for efficient transport and fusion of lysosomes. In low-cholesterol conditions (right panel), the cholesterol-binding domain of ORP1L is released from late endosomal membranes and exposes its FFAT domain for binding ER protein VAP-A. This terminates binding of the HOPS complex as well as p150^{Glued} to RILP. This mechanism shows how late endosomal cholesterol controls transport and fusion mediated by the complex of OPR1L, RAB7, RILP, dynein motor and HOPS.

recruitment. These may reflect multiple non-overlapping RILP binding sites in the mammalian HOPS complex, as has been recently shown for Ytp7 and the yeast HOPS complex (Bröcker et al., 2012). Mutations of RILP that abrogate HOPS complex recruitment also affect dynein motor recruitment and the C-terminus of p150^{Glued} increases the affinity of binding of RAB7–RILP in SPR studies with purified proteins. This suggests that HOPS is an integral part of the RAB7–RILP–p150^{Glued} complex (as the total has the highest affinity) and that minus-end transport and tethering for fusion are coupled processes. Such interplay between the dynein motor and HOPS complex could explain endosomal clustering near the MTOC observed upon overexpression of HOPS complex subunits (Caplan et al., 2001; Poupon et al., 2003). In these studies exogenous HOPS subunits were also observed on LE at steady state levels. We did not observe this, even when endogenous VPS11 was replaced by tagged VPS11 expressed at endogenous levels (Fig. 1E), possibly indicating differences in the amount of recruitment machinery present between different cell lines. Recently, another GTPase, ARL8b, was shown to recruit HOPS subunit VPS41 to lysosomal membranes (Garg et al., 2011). Arl8 also binds the kinesin-1 linker SKIP, thereby regulating anterograde trafficking (Rosa-Ferreira and Munro, 2011). Whether these two processes are coupled, as in the case for RAB7–RILP, or mutually exclusive, remains to be established. ARL8b and RILP localise to different endosomes (our unpublished data), suggesting that they may act in different steps of endosomal trafficking as suggested before (Garg et al., 2011).

The timing of vesicle tethering has to be well coordinated in time and space to ensure for correct fusion. We observed that HOPS complex subunits under steady state conditions were predominantly localized in the cytosol. This might indicate that the association of HOPS complex with membranes is very transient and/or regulated by other factors such as phosphorylation or lipid conditions. Regulation of the HOPS complex by phosphorylation has been reported before (Ruan et al., 2010; Cabrera et al., 2010) and we have previously shown that the recruitment of the dynein motor to RAB7–RILP is regulated and timed by the late endosomal cholesterol sensor ORP1L (Rocha et al., 2009). At high cholesterol concentrations, ORP1L allows binding of the dynein motor to RAB7–RILP. ORP1L changes conformation at low cholesterol concentrations and exposes an FFAT motif to interact with the ER protein VAP-A. VAP-A removes the dynein motor from RAB7–RILP complexes and vesicles relocalize to the cell periphery. We now show that endosomal tethering via the HOPS complex is also controlled by cholesterol sensor ORP1L. ORP1L seems to act as a molecular switch, coordinating vesicle movement and tethering dependent on late endosomal content (cholesterol) (Fig. 6).

As RILP coordinates vesicular tethering, it might modulate infectivity of pathogens entering the host via the endo-lysosomal pathway. For instance, *Salmonella* replicates in endosomes but avoids fusion with the degradative (phago)lysosome. Overexpression of RILP breaks this block and severely compromises intracellular bacterial infection (Guignot et al., 2004; Harrison et al., 2004; Marsman et al., 2004). Conversely, efficient delivery into late endosomes and lysosomes is essential for successful infection of Ebola virus by fusion and subsequent entry into the host cytosol. Here we show that RILP and ORP1L regulate fusion and infection by the Ebola virus. Various viruses including Dengue, influenza and HIV also have been reported to require late endosomal compartments for proper infectivity and propagation (van der Schaar et al., 2008; Caillet et al., 2011; Sieczkarski and Whittaker, 2003) and HIV propagation involves RILP as well (Lehmann et al., 2009; Lévesque et al., 2006). Whether late endosomal transport and tethering by RILP–HOPS–dynein is indeed important for host cell infection with these viruses remains to be determined.

VPS33b and SPE-39 have previously been reported to interact with RAB11A (Cullinane et al., 2010), a RAB GTPase present on recycling endosomes. Recyling endosomes have been implicated in epithelial polarization, and defective endosomal recycling might cause the abnormalities observed in polarized kidney and liver cells of ARC syndrome patients (Cullinane et al., 2010). We show that VPS33b and SPE-39 can also be recruited by RILP and that a disease mutant of VPS33b (VPS33b L30P) that causes severe ARC phenotype fails to be recruited to RILP. Our data suggest that VPS33b and SPE-39 might also have a role later in the endosomal pathway of mammalian cells.

Many cellular transport steps rely on dynein motor activity for transport and on multi-subunit tethering complexes for initiation of fusion (Stenmark, 2009; Bröcker et al., 2010) but the connection between these was unclear. We hypothesize that during evolution, organelles in higher eukaryotes may have required additional factors to recruit and time long-distance transport machineries, in addition to the tethering machinery. For late endosomes this is

reflected by two additional RAB7 effectors not found in yeast; RILP and ORP1L. These additional effectors might have interfered with existing RAB7 – HOPS interactions and this, in addition with the loss of the membrane binding motif in VPS41, might have required new interactions for membrane recruitment of the HOPS complex. This problem may have been solved by involving the RAB7-effector RILP (or a shared surface of RAB7–RILP) in HOPS recruitment which, at the same time, also provides cells with an efficient way of coupling transport and tethering and allowing co-regulation by the cholesterol senor ORP1L. Whether transport and fusion processes are intricately coupled for other intracellular structures as well, remains to be determined.

Here, we have shown that the RAB7 effector RILP recruits protein complexes involved in two different but consecutive processes: the dynein–dynactin motor for minus-end transport of late endosomes and the HOPS complex for tethering for fusion of late endosomes and lysosomes. The cholesterol sensor ORP1L controls the timing of these processes, providing an additional layer of regulation (Fig. 6). Coupling these processes efficiently prepares incoming maturing vesicles for subsequent tethering and fusion steps. This provides cells with an efficient way of cargo delivery, as exemplified here by Ebola glycoprotein containing viral entry into the host cytosol from late endosomal compartments.

Materials and Methods

Constructs and cloning

RAB7, RILP, ORP1L, $p150^{Glued}$ and $p50^{dynamitin}$ constructs have been described previously (Rocha et al., 2009; Jordens et al., 2001). GFP–VPS16 and GFP–VPS18 were gifts from Chengyu Liang (Liang et al., 2008) (Department of Molecular Microbiology and Immunology, University of Southern California, Los Angeles). Generation of other constructs is described below.

V5-VPS16 was generated by PCR using primerset1 (supplementary material Table S1) and inserted into the HINDIII – EcoR1 sites in pcDNA3.1. VPS18 was subcloned into the Xho1-EcoR1 sites of a 2FLAG-C1 vector. VPS33a was a gift of V. Faundez. VPS39 was a gift of J. Bonifacino (National Institutes of Health, Bethesda, MD) and was subcloned into an mRFP-C1 vector. Tag-VPS33b was generated by PCR (IMAGE CLONE 3449387) using primerset2 and was inserted into the EcoR1 sites of mGFP-C1, mCHERRY-C1 and 2MYC-C1 Image vectors. Tag-VPS41 was generated by PCR (IMAGE CLONE 4822048) using primerset3 and was inserted into the BamH1 sites of mGFP-C1, mCHERRY-C1 and 2HA-C1. VPS11 was generated by PCR (IMAGE CLONE 6144541) using primerset 4 and was inserted into the EcoR1 site of mGFP-C1 or mCherry-C1. Spe-39/C14orf133-Tag was generated by PCR (IMAGE CLONE 3920459) using primerset5 (fwd) and was inserted into the EcoR1 and BamH1 sites of mGFP-N1 or mCHERRY-N1. Spe-39-HA was generated by PCR using primerset6 and was inserted into the BamH1 and EcoR1 sites of a pcDNA3.1 vector.

Point mutants of RILP were generated by PCR using these respective primer sets; RILP E178R primerset7, RILP R159EH160E primerset8, RILP D125RE126R primerset9, RILP E93RE94R primerset 10, RILP E66R primerset11, RILP R60E primerset12, RILP E38R primerset13, RILP Y26A primerset14.

Reagents

Rabbit anti-GFP and rabbit anti-mRFP antibodies were generated at home using purified His–mRFP or His–GFP recombinant proteins, respectively. Cross-reactivity has been excluded by Western blot analyses with various mRFP- or GFP-labelled fusion proteins. Other antibodies used were: mouse anti-CD63 (Vennegoor et al., 1985), mouse anti-γ-tubulin (Sigma) mouse anti-V5 and anti-V5-HRP (Invitrogen), anti-Myc and anti-Myc-HRP (Novus), anti-HA (Roche) and anti-HA–HRP (Abcam), anti-FLAG (M2) and anti-FLAG–HRP (Sigma) anti-VPS33A (C1C3) (GeneTex), anti-VPS33b (Proteintech), anti-VPS11 (Proteintech), anti-VPS41 (Proteintech), anti-VPS16 (Proteintech), anti-dynein intermediate chain (Sigma, clone 70.1), anti-GAPDH (Sigma), Anti-SPE-39 was a gift of V. Faundez (Center for Translational Social Neuroscience, Emory University, Atlanta). Fluorescent and HRP-conjugated secondary antibodies were obtained from Invitrogen. GST–VPS18 (aa 1–580) and GST–VPS41 (full length) protein (produced in an *in vitro* wheat germ expression system) were purchased from Abnova. GTP-γS was purchased from Millipore.

Protein purification

His–RAB7Q76L, His–RILP and MBP–C25 were produced as previously described (Johansson et al., 2007; Rocha et al., 2009). Cells were lysed in 0.5% Triton X-100, 20 mM Hepes, pH 7.5, 200 mM NaCl, 8 mM β-mercaptoethanol and complete EDTA-free protease inhibitor cocktail (Roche). The lysate was cleared by centrifugation and the supernatant was incubated with pre-equilibrated Talon Co^{2+} resin (Clontech Laboratories, Inc.) or MBP beads (New England Biolabs) for 30 minutes. The resin was washed extensively with 20 mM HEPES pH 7.5, 200 mM NaCl and 8 mM β-mercaptoethanol. Proteins were aliquoted and stored at −80℃ until used for protein reconstitution experiments.

Surface plasmon resonance

Binding assays were performed using Biacore T200 (GE). A CM5 Chip was coated with goat α-GST antibodies, and subsequently GST-tagged VPS proteins were immobilized in separate flow cells whereas GST protein alone was immobilized in a reference flow cell. Increasing concentrations of the analyte proteins were sequentially injected over the Chip surface. Analysis of the data was done using Biacore T200 Evaluation Software (GE). Association constants were calculated using the equilibrium SPR response levels for each analyte concentration. Fitting of affinity constants and final figures applied Graphpad Prism (GraphPad Software, La Jolla, California, USA, http://www.graphpad.com).

Gel filtration

Transfected Meljuso cells were washed with ice-cold PBS and scraped into buffer (50 mM Tris, 150 mM NaCl, 5 mM $MgCl_2$, pH 7.4) supplemented with complete EDTA-free protease inhibitor cocktail. Cells were lysed by using the EMBL 8.020 mm 'cell cracker' homogenizer (ball sizes 8.010, 15 times) followed by a centrifugation for clearing membranes and nuclei. In experiments with recombinant proteins, untransfected MelJuso cells were used and indicated recombinant proteins were mixed with the lysate for 30 minutes at 4℃. All supernatants were loaded onto a Superose 6 10/300 column connected to an Åkta purifier system (GE Healthcare). The column was equilibrated with running buffer (25 mM Tris-HCl pH 7.5, 150 mM NaCl) and the flow-rate of the column was set at 0.2–0.3 ml/minute. Fractions (1 ml) were collected and analysed by SDS-PAGE and western blotting with the indicated antibodies. Protein (complex) molecular masses were calculated by comparison of the respective elution volumes with protein markers with molecular masses ranging from 75 to 2000 kDa.

Melting curves

His–RAB7 and His–RILP were co-incubated in the presence of 100 μM GTP-γS and melting curves were determined using SYPRO® Orange dye in MyiQ real-time PCR detection system (Biorad).

Transfection

Expression constructs were transfected using Effectene reagents (Qiagen) according to manufacturer's instructions. For silencing, cells were transfected with Dharmafect1 (Thermo Fisher Scientific) with siRNA's (ON-TARGETplus SMARTpool) against VPS16, VPS33b, VPS33a, VPS11, Dynein Heavy Chain or control siRNA (Thermo Fisher Scientific).

Cell culture and microscopy

MelJuSo cells were cultured in Iscove's modified Dulbecco's medium (IMDM; Invitrogen) supplemented with 8% FCS in a 5% CO_2 humidified culture hood at 37℃. All specimens were analyzed by confocal laser-scanning microscopes (CLSM, TCS-SP1, TCS-SP2, or AOBS; Leica) equipped with HCX Plan-Apochromat 63× NA 1.32 and HCX Plan-Apochromat lbd.bl 63×NA 1.4 oil-corrected objective lenses (Leica). The acquisition software used was LCS (Leica). For electron microscopy a CM10 electron microscope (FEI, Eindhoven, the Netherlands) was used.

Protein immunoprecipitation

MelJuSo cells were washed with ice-cold PBS and scraped into cell lysis buffer (50 mM Tris-HCl, 150 mM NaCl, 5 mM $MgCl_2$, 1% NP40, 10% glycerol, pH 7.4) supplemented with complete EDTA-free Protease Inhibitor Cocktail. Cell lysates were obtained by incubation on ice for 10 minutes followed by centrifugation for clearing. The supernatants were incubated for 2 hours with respective antibodies followed by capture with protein-G–Sepharose-4 FF resin and washed extensively with wash-buffer (50 mM Tris-HCl, 150 mM NaCl, 5 mM $MgCl_2$, 10% glycerol, pH 7.4). For GFP-tagged pull-down, GFP-TRAP beads were used (Chromotek).

Microscopy sample preparation

Transfected cells were fixed 24 hours post-transfection with ice-cold methanol (Fig. 1A,B) or 4% formaldehyde (all other figures) in PBS for 30 minutes and formaldehyde-fixed samples were permeabilized for 5 minutes with 0.05% Triton X-100 in PBS at room temperature. Non-specific binding of antibodies was blocked by 0.5%BSA in PBS for 40 minutes, after which cells were incubated with primary antibodies in 0.5%BSA in PBS for 1 hour at room temperature. Bound primary antibodies were visualized with Alexa-Fluor secondary antibody conjugates (Invitrogen). Cells were mounted in Vectashield mounting medium (Vector Laboratories).

VPS11 rescue experiment

Haploid Hap1 cells knockout for VPS11(Carette et al., 2011) were cultured in Iscove's modified Dulbecco's medium (IMDM; Invitrogen) supplemented with 8% FCS. Cells were electroporated with GFP–VPS11 and mRFP–VPS11 or mRFP–VPS11 in combination with GFP–RILP, or GFP–RILPΔ199 and, after 24 hours, fixed with 4% formaldehyde in PBS for 30 minutes and mounted in Vectashield mounting medium (Vector Laboratories). The slides were analyzed by confocal laser-scanning microscopes.

Immunoelectron microscopy

Cells were fixed in 2% paraformaldehyde + 0.2% glutaraldehyde in 0.1 M PHEM buffer (60 mM Pipes, 25 mM Hepes, 2 mM $MgCl_2$ and 10 mM EGTA, pH 6.9) and then processed for ultrathin cryosectioning. 50 nm-thick cryosections were cut at −120℃ using diamond knives in a cryo-ultramicrotome (Leica, Vienna) and transferred with a mixture of sucrose and methylcellulose onto formvar-coated copper grids. The grids were placed on 35-mm 2% gelatin plates at 37℃. The grids were incubated with the various antibodies at room temperature and then incubated with 10 nm protein A–conjugated colloidal gold (EM Laboratory, Utrecht University). After immunolabelling, the sections were embedded in a mixture of methylcellulose and 0.6% uranylacetate and examined by a CM10 electron microscope (FEI, Eindhoven, the Netherlands) (Calafat et al., 1997).

Epon embedding

Cultured cells were fixed in Karnovsky fixative. To increase contrast, a post-fixation step with 1% Osmiumtetroxide in 0.1 M cacodylatebuffer was performed. After washing, the pellets were stained *en bloc* with Ultrastain 1 (Leica, Vienna, Austria) followed by an ethanol dehydration series. Finally, the cells were embedded in a mixture of DDSA/NMA/Embed-812 (EMS, Hatfield, U.S.A.), sectioned and stained with Ultrastain 1 and Ultrastain 2 (Leica, Vienna, Austria) before analysis by a CM10 electron microscope.

Ebola-VSV infection

Haploid wildtype Hap1 cells (Carette et al., 2011) were cultured in Iscove's modified Dulbecco's medium (IMDM; Invitrogen) supplemented with 8% FCS. Cells were electroporated with mRFP, mRFP–RILP or mRFP–RILP D125RE125R expression constructs. 24 hours post-transfection, the cells were exposed to rVSV-GP-EboV at MOI ~100 for 8 hours. 8 hours post-infection, cells were fixed with 4% formaldehyde and prepared for analysis by confocal microscopy or flow cytometry. 8 hours post-infection, cells were fixed with 4% formaldehyde in PBS for 30 minutes and mounted in Vectashield mounting medium (Vector Laboratories), as described above. The specimens were analyzed by confocal laser-scanning microscopes equipped with HCX Plan-Apochromat 63×NA 1.32 and HCX Plan-Apochromat lbd.bl 63×NA 1.4 oil-corrected objective lenses (Leica). The acquisition software used was LCS (Leica). All images were taken with identical settings. For quantification, we selected transfected (marked by mRFP) cells and determined infection by rVSV-GP-EboV (marked by GFP expressed by the virus).

In order to visualize and quantify single and double fluorescent cells in our Ebola-VSV infection experiment (masked overlays), we used CellProfiler (http://www.cellprofiler.org) to detect and mask cells in the red and the green channel, which were subsequently overlaid to create the masked merged images. For flow cytometry analysis, the transfection and infection protocol was identical. Cells were harvested by trypsinization and fixed with 4% formaldehyde in PBS for 30 minutes. Cells were analyzed on a BD LSR II flow cytometer (BD Biosciences) using FACSDiva software(BD Biosciences) using appropriate settings to detect GFP and RFP.

Statistical analysis

For calculation of correlation coefficients the signal intensity over a vector was plotted using the plot profile tool in ImageJ (http://imagej.nih.gov/ij/index.html) in both the green and red channel. Correlation coefficients for the two plots were calculated in Excel using the function:

$$Correl(X,Y)=\frac{\sum(x-\bar{x})(y-\bar{y})}{\sqrt{\sum(x-\bar{x})^2\sum(y-\bar{y})^2}}$$

For Fig. 3B, statistics were performed in GraphPad Prism using one-way ANOVA followed by Bonferroni's post-hoc comparisons tests. All other statistics were performed in Microsoft Excel using a two sided Student's *t*-test.

Acknowledgements

We thank C. Liang, J. Bonifacino, V. Faundez, S. Zlatic and J. Hoogenraad for providing reagents and our colleagues at the 2012 Gordon Conference on Lysosomes for discussions, M. Garstka for primer design, R. Spaapen for FACS and statistical analyses, N. Ong for processing electron micrographs, P. Celie and M. Stadnik-Spiewak for protein production and gel filtration, I. Zondervan, W. Wong, A. Jaramillo and R. Ligthart for helping with experiments and I. Berlin for reading the manuscript.

Author contributions

R.v.d.K. designed and performed experiments, analysed data and wrote the paper; A.F. performed SPR experiments; L.J., S.K and N.N assisted with experiments; H.J. performed electron microscopy; T.B. and J.C. performed Ebola-VSV experiments; N.R. designed and performed experiments; and J.N. designed experiments and wrote the paper.

Funding

This work is supported by a European Research Council Advanced Grant; and a TOP grant from The Netherlands Organisation for Scientific Research – Chemical Sciences.

Supplementary material available online at
http://jcs.biologists.org/lookup/suppl/doi:10.1242/jcs.129270/-/DC1

References

Aoyama, M., Sun-Wada, G. H., Yamamoto, A., Yamamoto, M., Hamada, H. and Wada, Y. (2012). Spatial restriction of bone morphogenetic protein signaling in mouse gastrula through the mVam2-dependent endocytic pathway. *Dev. Cell* **22**, 1163-1175.

BasuRay, S., Mukherjee, S., Romero, E. G., Seaman, M. N. and Wandinger-Ness, A. (2013). Rab7 mutants associated with Charcot-Marie-Tooth disease cause delayed growth factor receptor transport and altered endosomal and nuclear signaling. *J. Biol. Chem.* **288**, 1135-1149.

Bröcker, C., Engelbrecht-Vandré, S. and Ungermann, C. (2010). Multisubunit tethering complexes and their role in membrane fusion. *Curr. Biol.* **20**, R943-R952.

Bröcker, C., Kuhlee, A., Gatsogiannis, C., Balderhaar, H. J., Hönscher, C., Engelbrecht-Vandré, S., Ungermann, C. and Raunser, S. (2012). Molecular architecture of the multisubunit homotypic fusion and vacuole protein sorting (HOPS) tethering complex. *Proc. Natl. Acad. Sci. U S A.* **109**, 1991-1996.

Cabrera, M., Ostrowicz, C. W., Mari, M., LaGrassa, T. J., Reggiori, F. and Ungermann, C. (2009). Vps41 phosphorylation and the Rab Ypt7 control the targeting of the HOPS complex to endosome-vacuole fusion sites. *Mol. Biol. Cell* **20**, 1937-1948.

Cabrera, M., Langemeyer, L., Mari, M., Rethmeier, R., Orban, I., Perz, A., Bröcker, C., Griffith, J., Klose, D., Steinhoff, H. J. et al. (2010). Phosphorylation of a membrane curvature-sensing motif switches function of the HOPS subunit Vps41 in membrane tethering. *J. Cell Biol.* **191**, 845-859.

Caillet, M., Janvier, K., Pelchen-Matthews, A., Delcroix-Genête, D., Camus, G., Marsh, M. and Berlioz-Torrent, C. (2011). Rab7A is required for efficient production of infectious HIV-1. *PLoS Pathog.* **7**, e1002347.

Calafat, J., Janssen, H., Knol, E. F., Weller, P. F. and Egesten, A. (1997). Ultrastructural localization of Charcot-Leyden crystal protein in human eosinophils and basophils. *Eur. J. Haematol.* **58**, 56-66.

Cantalupo, G., Alifano, P., Roberti, V., Bruni, C. B. and Bucci, C. (2001). Rab-interacting lysosomal protein (RILP): the Rab7 effector required for transport to lysosomes. *EMBO J.* **20**, 683-693.

Caplan, S., Hartnell, L. M., Aguilar, R. C., Naslavsky, N. and Bonifacino, J. S. (2001). Human Vam6p promotes lysosome clustering and fusion in vivo. *J. Cell Biol.* **154**, 109-122.

Carette, J. E., Raaben, M., Wong, A. C., Herbert, A. S., Obernosterer, G., Mulherkar, N., Kuehne, A. I., Kranzusch, P. J., Griffin, A. M., Ruthel, G. et al. (2011). Ebola virus entry requires the cholesterol transporter Niemann-Pick C1. *Nature* **477**, 340-343.

Chirivino, D., Del Maestro, L., Formstecher, E., Hupé, P., Raposo, G., Louvard, D. and Arpin, M. (2011). The ERM proteins interact with the HOPS complex to regulate the maturation of endosomes. *Mol. Biol. Cell* **22**, 375-385.

Christoforidis, S., McBride, H. M., Burgoyne, R. D. and Zerial, M. (1999). The Rab5 effector EEA1 is a core component of endosome docking. *Nature* **397**, 621-625.

Cullinane, A. R., Straatman-Iwanowska, A., Zaucker, A., Wakabayashi, Y., Bruce, C. K., Luo, G., Rahman, F., Gürakan, F., Utine, E., Ozkan, T. B. et al. (2010). Mutations in VIPAR cause an arthrogryposis, renal dysfunction and cholestasis syndrome phenotype with defects in epithelial polarization. *Nat. Genet.* **42**, 303-312.

Daniele, T., Hackmann, Y., Ritter, A. T., Wenham, M., Booth, S., Bossi, G., Schintler, M., Auer-Grumbach, M. and Griffiths, G. M. (2011). A role for Rab7 in the movement of secretory granules in cytotoxic T lymphocytes. *Traffic* **12**, 902-911.

Ganley, I. G., Wong, P. M., Gammoh, N. and Jiang, X. (2011). Distinct autophagosomal-lysosomal fusion mechanism revealed by thapsigargin-induced autophagy arrest. *Mol. Cell* **42**, 731-743.

Garg, S., Sharma, M., Ung, C., Tuli, A., Barral, D. C., Hava, D. L., Veerapen, N., Besra, G. S., Hacohen, N. and Brenner, M. B. (2011). Lysosomal trafficking,

antigen presentation, and microbial killing are controlled by the Arf-like GTPase Arl8b. *Immunity* **35**, 182-193.

Gissen, P., Johnson, C. A., Morgan, N. V., Stapelbroek, J. M., Forshew, T., Cooper, W. N., McKiernan, P. J., Klomp, L. W., Morris, A. A., Wraith, J. E. et al. (2004). Mutations in VPS33B, encoding a regulator of SNARE-dependent membrane fusion, cause arthrogryposis-renal dysfunction-cholestasis (ARC) syndrome. *Nat. Genet.* **36**, 400-404.

Gissen, P., Johnson, C. A., Gentle, D., Hurst, L. D., Doherty, A. J., O'Kane, C. J., Kelly, D. A. and Maher, E. R. (2005). Comparative evolutionary analysis of VPS33 homologues: genetic and functional insights. *Hum. Mol. Genet.* **14**, 1261-1270.

Guignot, J., Caron, E., Beuzón, C., Bucci, C., Kagan, J., Roy, C. and Holden, D. W. (2004). Microtubule motors control membrane dynamics of Salmonella-containing vacuoles. *J. Cell Sci.* **117**, 1033-1045.

Harrington, A. J., Yacoubian, T. A., Slone, S. R., Caldwell, K. A. and Caldwell, G. A. (2012). Functional analysis of VPS41-mediated neuroprotection in Caenorhabditis elegans and mammalian models of Parkinson's disease. *J. Neurosci.* **32**, 2142-2153.

Harrison, R. E., Brumell, J. H., Khandani, A., Bucci, C., Scott, C. C., Jiang, X., Finlay, B. B. and Grinstein, S. (2004). Salmonella impairs RILP recruitment to Rab7 during maturation of invasion vacuoles. *Mol. Biol. Cell* **15**, 3146-3154.

Hoepfner, S., Severin, F., Cabezas, A., Habermann, B., Runge, A., Gillooly, D., Stenmark, H. and Zerial, M. (2005). Modulation of receptor recycling and degradation by the endosomal kinesin KIF16B. *Cell* **121**, 437-450.

Huizing, M., Didier, A., Walenta, J., Anikster, Y., Gahl, W. A. and Krämer, H. (2001). Molecular cloning and characterization of human VPS18, VPS 11, VPS16, and VPS33. *Gene* **264**, 241-247.

Johansson, M., Rocha, N., Zwart, W., Jordens, I., Janssen, L., Kuijl, C., Olkkonen, V. M. and Neefjes, J. (2007). Activation of endosomal dynein motors by stepwise assembly of Rab7-RILP-p150Glued, ORP1L, and the receptor betalll spectrin. *J. Cell Biol.* **176**, 459-471.

Jordens, I., Fernandez-Borja, M., Marsman, M., Dusseljee, S., Janssen, L., Calafat, J., Janssen, H., Wubbolts, R. and Neefjes, J. (2001). The Rab7 effector protein RILP controls lysosomal transport by inducing the recruitment of dynein-dynactin motors. *Curr. Biol.* **11**, 1680-1685.

Jordens, I., Westbroek, W., Marsman, M., Rocha, N., Mommaas, M., Huizing, M., Lambert, J., Naeyaert, J. M. and Neefjes, J. (2006). Rab7 and Rab27a control two motor protein activities involved in melanosomal transport. *Pigment Cell Res.* **19**, 412-423.

Kuijl, C., Savage, N. D., Marsman, M., Tuin, A. W., Janssen, L., Egan, D. A., Ketema, M., van den Nieuwendijk, R., van den Eeden, S. J., Geluk, A. et al. (2007). Intracellular bacterial growth is controlled by a kinase network around PKB/AKT1. *Nature* **450**, 725-730.

Lehmann, M., Milev, M. P., Abrahamyan, L., Yao, X. J., Pante, N. and Mouland, A. J. (2009). Intracellular transport of human immunodeficiency virus type 1 genomic RNA and viral production are dependent on dynein motor function and late endosome positioning. *J. Biol. Chem.* **284**, 14572-14585.

Lévesque, K., Halvorsen, M., Abrahamyan, L., Chatel-Chaix, L., Poupon, V., Gordon, H., DesGroseillers, L., Gatignol, A. and Mouland, A. J. (2006). Trafficking of HIV-1 RNA is mediated by heterogeneous nuclear ribonucleoprotein A2 expression and impacts on viral assembly. *Traffic* **7**, 1177-1193.

Liang, C., Lee, J. S., Inn, K. S., Gack, M. U., Li, Q., Roberts, E. A., Vergne, I., Deretic, V., Feng, P., Akazawa, C. et al. (2008). Beclin1-binding UVRAG targets the class C Vps complex to coordinate autophagosome maturation and endocytic trafficking. *Nat. Cell Biol.* **10**, 776-787.

Marsman, M., Jordens, I., Kuijl, C., Janssen, L. and Neefjes, J. (2004). Dynein-mediated vesicle transport controls intracellular Salmonella replication. *Mol. Biol. Cell* **15**, 2954-2964.

Ostrowicz, C. W., Bröcker, C., Ahnert, F., Nordmann, M., Lachmann, J., Peplowska, K., Perz, A., Auffarth, K., Engelbrecht-Vandré, S. and Ungermann, C. (2010). Defined subunit arrangement and rab interactions are required for functionality of the HOPS tethering complex. *Traffic* **11**, 1334-1346.

Paul, P., van den Hoorn, T., Jongsma, M. L., Bakker, M. J., Hengeveld, R., Janssen, L., Cresswell, P., Egan, D. A., van Ham, M., Ten Brinke, A. et al. (2011). A Genome-wide multidimensional RNAi screen reveals pathways controlling MHC class II antigen presentation. *Cell* **145**, 268-283.

Poupon, V., Stewart, A., Gray, S. R., Piper, R. C. and Luzio, J. P. (2003). The role of mVps18p in clustering, fusion, and intracellular localization of late endocytic organelles. *Mol. Biol. Cell* **14**, 4015-4027.

Pulipparacharuvil, S., Akbar, M. A., Ray, S., Sevrioukov, E. A., Haberman, A. S., Rohrer, J. and Krämer, H. (2005). Drosophila Vps16A is required for trafficking to lysosomes and biogenesis of pigment granules. *J. Cell Sci.* **118**, 3663-3673.

Raaijmakers, J. A., van Heesbeen, R. G., Meaders, J. L., Geers, E. F., Fernandez-Garcia, B., Medema, R. H. and Tanenbaum, M. E. (2012). Nuclear envelope-associated dynein drives prophase centrosome separation and enables Eg5-independent bipolar spindle formation. *EMBO J.* **31**, 4179-4190.

Rocha, N., Kuijl, C., van der Kant, R., Janssen, L., Houben, D., Janssen, H., Zwart, W. and Neefjes, J. (2009). Cholesterol sensor ORP1L contacts the ER protein VAP to control Rab7-RILP-p150 Glued and late endosome positioning. *J. Cell Biol.* **185**, 1209-1225.

Rosa-Ferreira, C. and Munro, S. (2011). Arl8 and SKIP act together to link lysosomes to kinesin-1. *Dev. Cell* **21**, 1171-1178.

Ruan, Q., Harrington, A. J., Caldwell, K. A., Caldwell, G. A. and Standaert, D. G. (2010). VPS41, a protein involved in lysosomal trafficking, is protective in Caenorhabditis elegans and mammalian cellular models of Parkinson's disease. *Neurobiol. Dis.* **37**, 330-338.

Sevrioukov, E. A., He, J. P., Moghrabi, N., Sunio, A. and Krämer, H. (1999). A role for the deep orange and carnation eye color genes in lysosomal delivery in Drosophila. *Mol. Cell* **4**, 479-486.

Sieczkarski, S. B. and Whittaker, G. R. (2003). Differential requirements of Rab5 and Rab7 for endocytosis of influenza and other enveloped viruses. *Traffic* **4**, 333-343.

Sobo, K., Le Blanc, I., Luyet, P. P., Fivaz, M., Ferguson, C., Parton, R. G., Gruenberg, J. and van der Goot, F. G. (2007). Late endosomal cholesterol accumulation leads to impaired intra-endosomal trafficking. *PLoS ONE* **2**, e851.

Spinosa, M. R., Progida, C., De Luca, A., Colucci, A. M., Alifano, P. and Bucci, C. (2008). Functional characterization of Rab7 mutant proteins associated with Charcot-Marie-Tooth type 2B disease. *J. Neurosci.* **28**, 1640-1648.

Stenmark, H. (2009). Rab GTPases as coordinators of vesicle traffic. *Nat. Rev. Mol. Cell Biol.* **10**, 513-525.

Uusi-Rauva, K., Kyttälä, A., van der Kant, R., Vesa, J., Tanhuanpää, K., Neefjes, J., Olkkonen, V. M. and Jalanko, A. (2012). Neuronal ceroid lipofuscinosis protein CLN3 interacts with motor proteins and modifies location of late endosomal compartments. *Cell. Mol. Life Sci.* **69**, 2075-2089.

Vallee, R. B., McKenney, R. J. and Ori-McKenney, K. M. (2012). Multiple modes of cytoplasmic dynein regulation. *Nat. Cell Biol.* **14**, 224-230.

van der Schaar, H. M., Rust, M. J., Chen, C., van der Ende-Metselaar, H., Wilschut, J., Zhuang, X. and Smit, J. M. (2008). Dissecting the cell entry pathway of dengue virus by single-particle tracking in living cells. *PLoS Pathog.* **4**, e1000244.

Vennegoor, C., Calafat, J., Hageman, P., van Buitenen, F., Janssen, H., Kolk, A. and Rümke, P. (1985). Biochemical characterization and cellular localization of a formalin-resistant melanoma-associated antigen reacting with monoclonal antibody NKI/C-3. *Int. J. Cancer* **35**, 287-295.

Vihervaara, T., Uronen, R. L., Wohlfahrt, G., Björkhem, I., Ikonen, E. and Olkkonen, V. M. (2011). Sterol binding by OSBP-related protein 1L regulates late endosome motility and function. *Cell. Mol. Life Sci.* **68**, 537-551.

Wickner, W. (2010). Membrane fusion: five lipids, four SNAREs, three chaperones, two nucleotides, and a Rab, all dancing in a ring on yeast vacuoles. *Annu. Rev. Cell Dev. Biol.* **26**, 115-136.

Wong, A. C., Sandesara, R. G., Mulherkar, N., Whelan, S. P. and Chandran, K. (2010). A forward genetic strategy reveals destabilizing mutations in the Ebolavirus glycoprotein that alter its protease dependence during cell entry. *J. Virol.* **84**, 163-175.

Wu, X., Wang, F., Rao, K., Sellers, J. R. and Hammer, J. A., 3rd (2002). Rab27a is an essential component of melanosome receptor for myosin Va. *Mol. Biol. Cell* **13**, 1735-1749.

Zhu, G. D., Salazar, G., Zlatic, S. A., Fiza, B., Doucette, M. M., Heilman, C. J., Levey, A. I., Faundez, V. and L'hernault, S. W. (2009). SPE-39 family proteins interact with the HOPS complex and function in lysosomal delivery. *Mol. Biol. Cell* **20**, 1223-1240.

S1 A

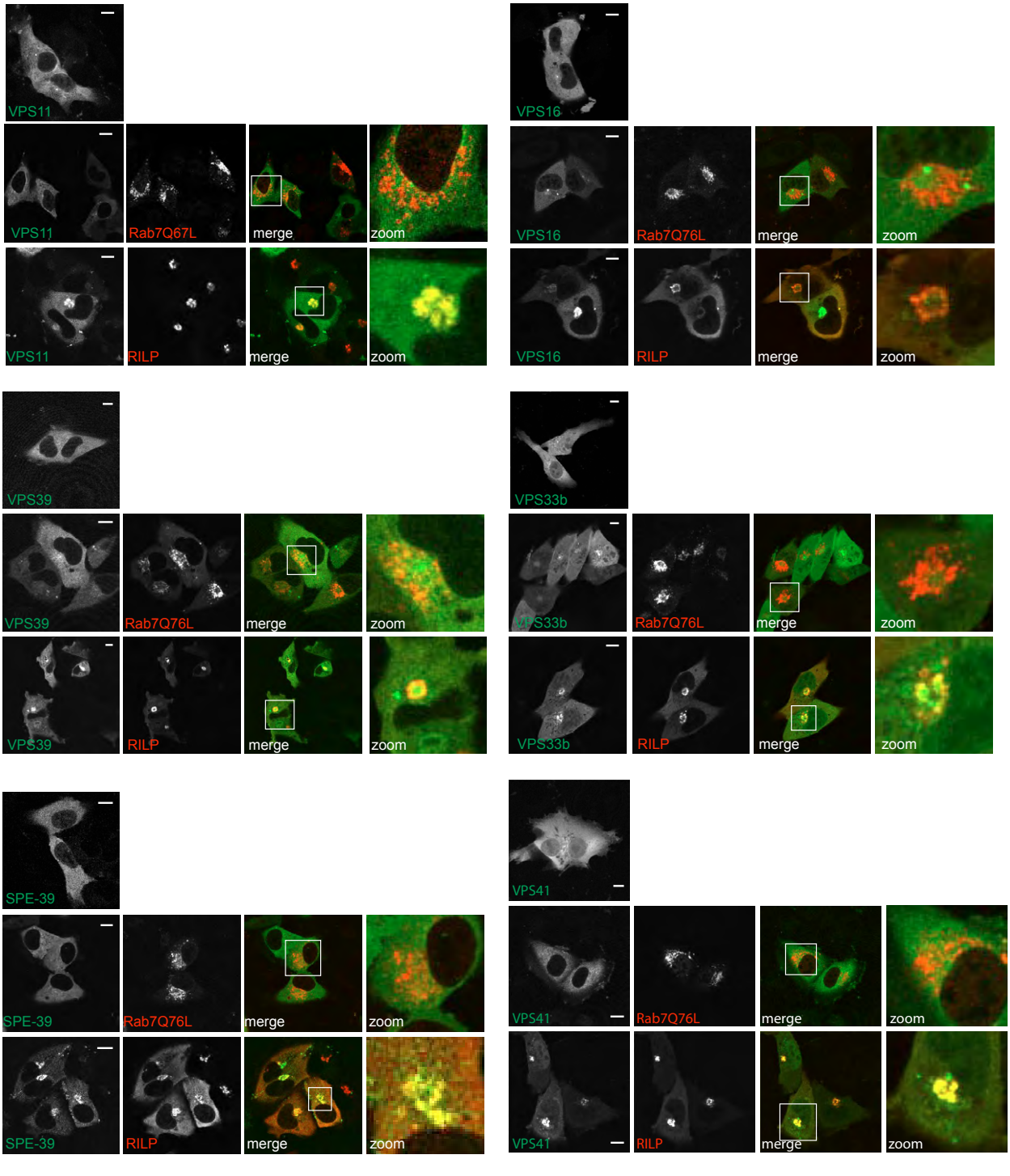
VPS11
VPS11
Rab7Q67L
merge
zoom
VPS11
RILP
merge
zoom
VPS16
VPS16
Rab7Q76L
merge
zoom
VPS16
RILP
merge
zoom
VPS39
VPS39
Rab7Q76L
merge
zoom
VPS39
RILP
merge
zoom
VPS33b
VPS33b
Rab7Q76L
merge
zoom
VPS33b
RILP
merge
zoom
SPE-39
SPE-39
Rab7Q76L
merge
zoom
SPE-39
RILP
merge
zoom
VPS41
VPS41
Rab7Q76L
merge
zoom
VPS41
RILP
merge
zoom

S1 B

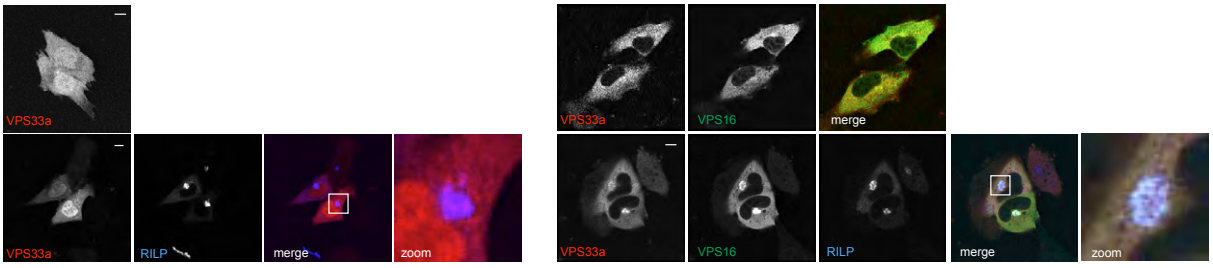
VPS33a
VPS33a
RILP
merge
zoom
VPS33a
VPS16
merge
VPS33a
VPS16
RILP
merge
zoom

S1 C

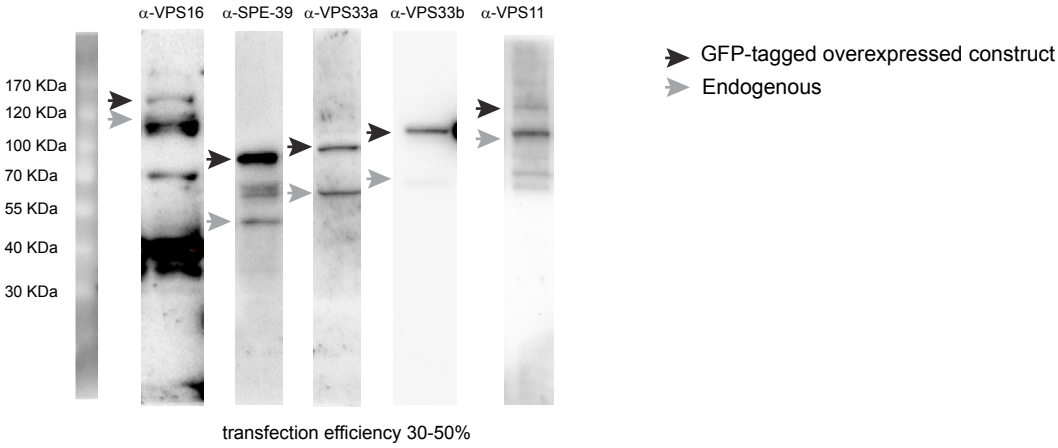
α-VPS16
α-SPE-39
α-VPS33a
α-VPS33b
α-VPS11
170 KDa
120 KDa
100 KDa
70 KDa
55 KDa
40 KDa
30 KDa
GFP-tagged overexpressed construct
Endogenous
transfection efficiency 30-50%

S1 D

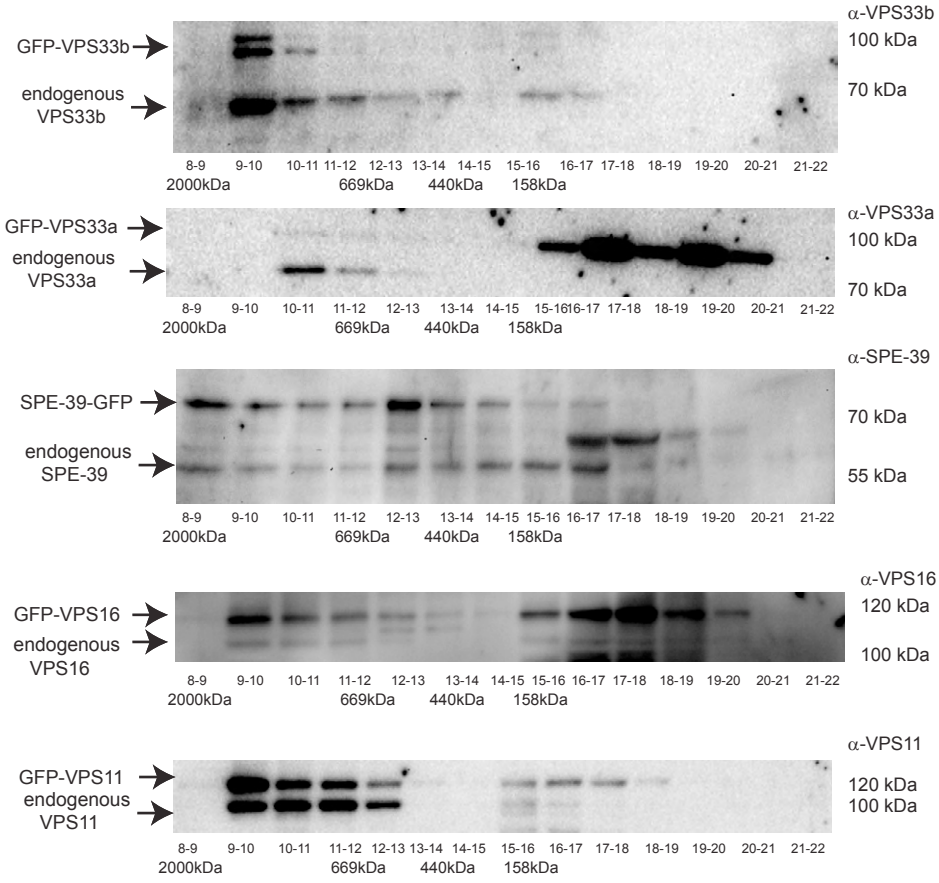
GFP-VPS33b
endogenous VPS33b
α-VPS33b
100 kDa
70 kDa
8-9 9-10 10-11 11-12 12-13 13-14 14-15 15-16 16-17 17-18 18-19 19-20 20-21 21-22
2000kDa 669kDa 440kDa 158kDa
GFP-VPS33a
endogenous VPS33a
α-VPS33a
100 kDa
70 kDa
8-9 9-10 10-11 11-12 12-13 13-14 14-15 15-16 16-17 17-18 18-19 19-20 20-21 21-22
2000kDa 669kDa 440kDa 158kDa
SPE-39-GFP
endogenous SPE-39
α-SPE-39
70 kDa
55 kDa
8-9 9-10 10-11 11-12 12-13 13-14 14-15 15-16 16-17 17-18 18-19 19-20 20-21 21-22
2000kDa 669kDa 440kDa 158kDa
GFP-VPS16
endogenous VPS16
α-VPS16
120 kDa
100 kDa
8-9 9-10 10-11 11-12 12-13 13-14 14-15 15-16 16-17 17-18 18-19 19-20 20-21 21-22
2000kDa 669kDa 440kDa 158kDa
GFP-VPS11
endogenous VPS11
α-VPS11
120 kDa
100 kDa
8-9 9-10 10-11 11-12 12-13 13-14 14-15 15-16 16-17 17-18 18-19 19-20 20-21 21-22
2000kDa 669kDa 440kDa 158kDa

S1E

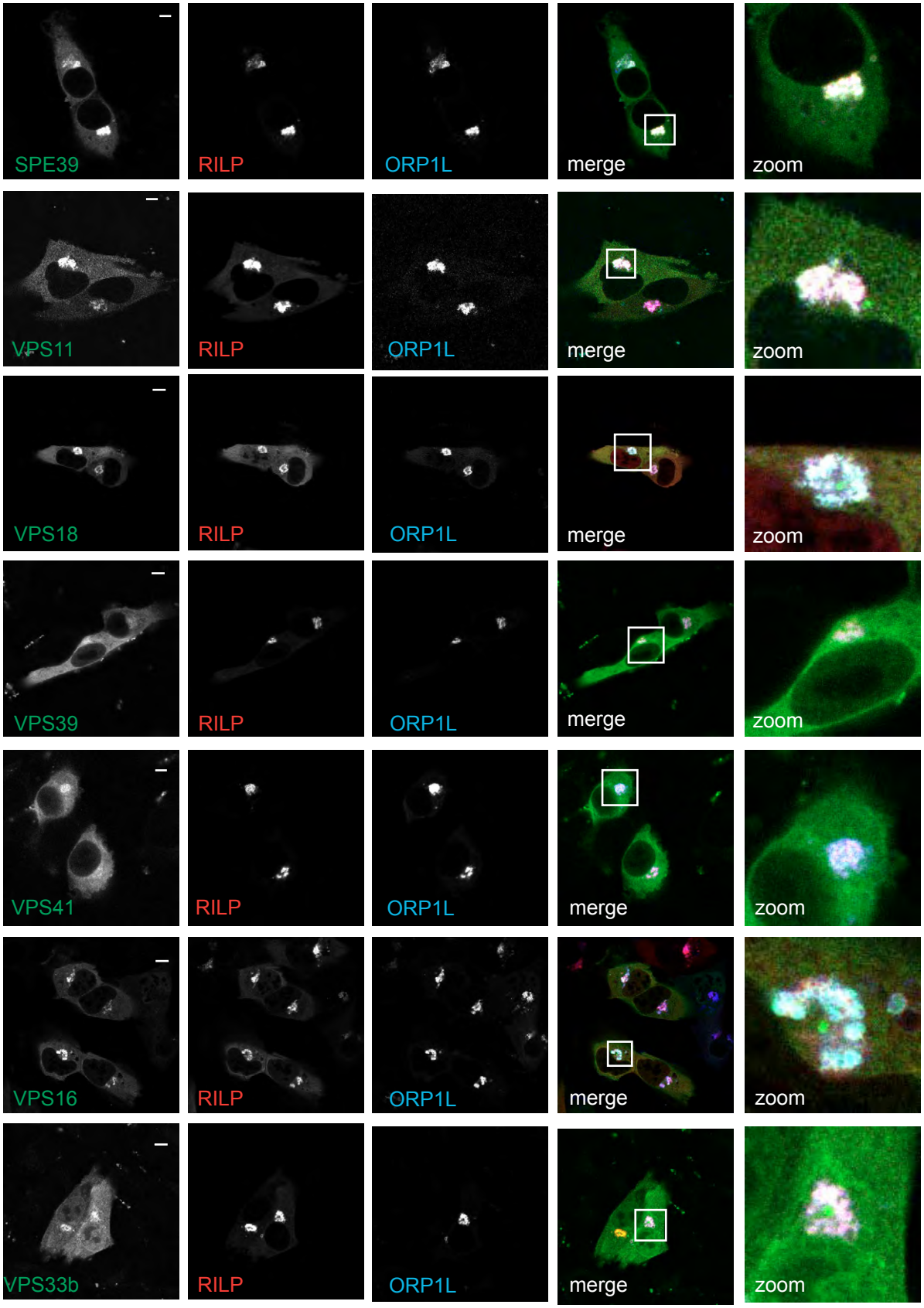
SPE39
RILP
ORP1L
merge
zoom
VPS11
RILP
ORP1L
merge
zoom
VPS18
RILP
ORP1L
merge
zoom
VPS39
RILP
ORP1L
merge
zoom
VPS41
RILP
ORP1L
merge
zoom
VPS16
RILP
ORP1L
merge
zoom
VPS33b
RILP
ORP1L
merge
zoom

S1F

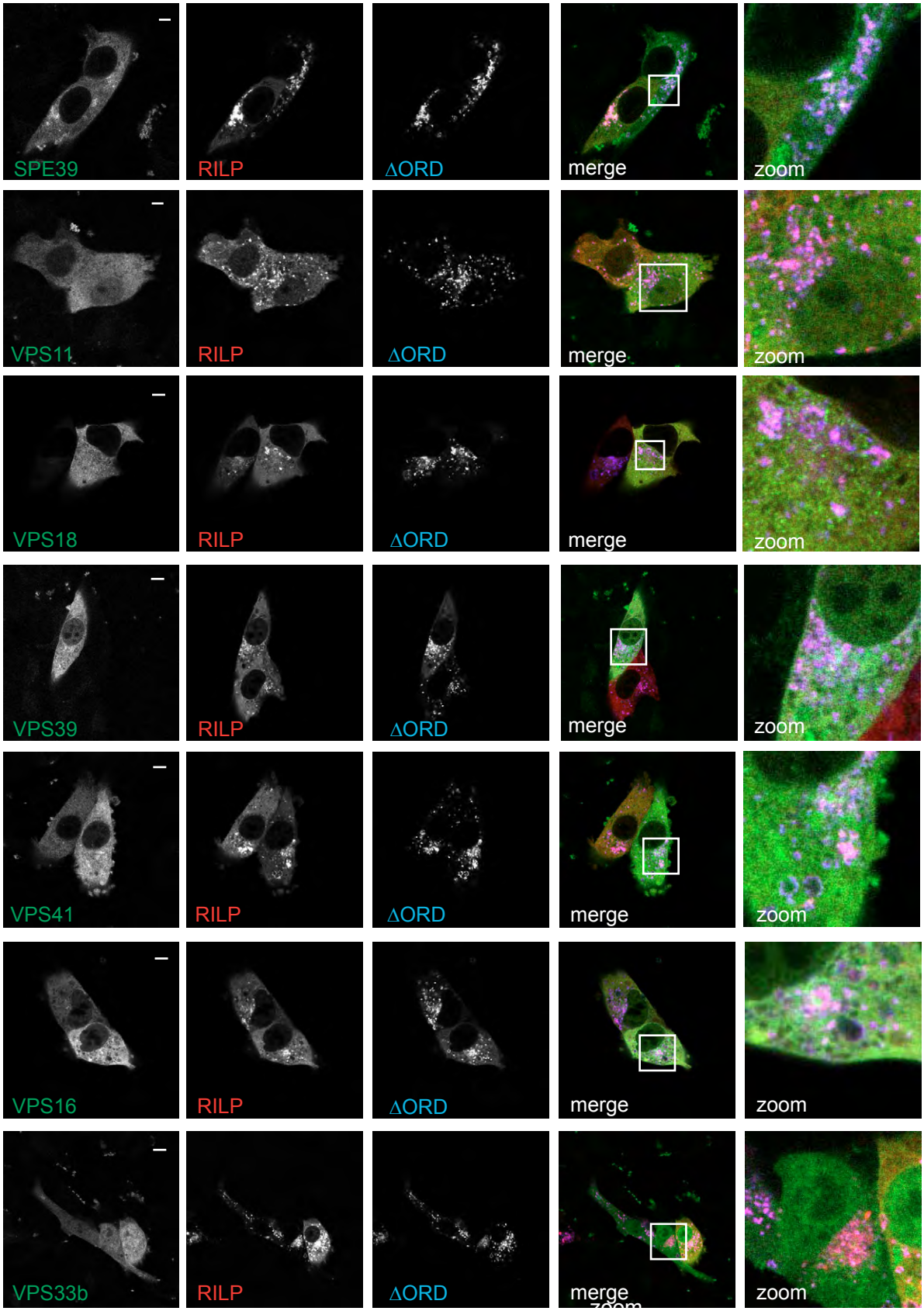
SPE39
RILP
ΔORD
merge
zoom
VPS11
RILP
ΔORD
merge
zoom
VPS18
RILP
ΔORD
merge
zoom
VPS39
RILP
ΔORD
merge
zoom
VPS41
RILP
ΔORD
merge
zoom
VPS16
RILP
ΔORD
merge
zoom
VPS33b
RILP
ΔORD
merge
zoom

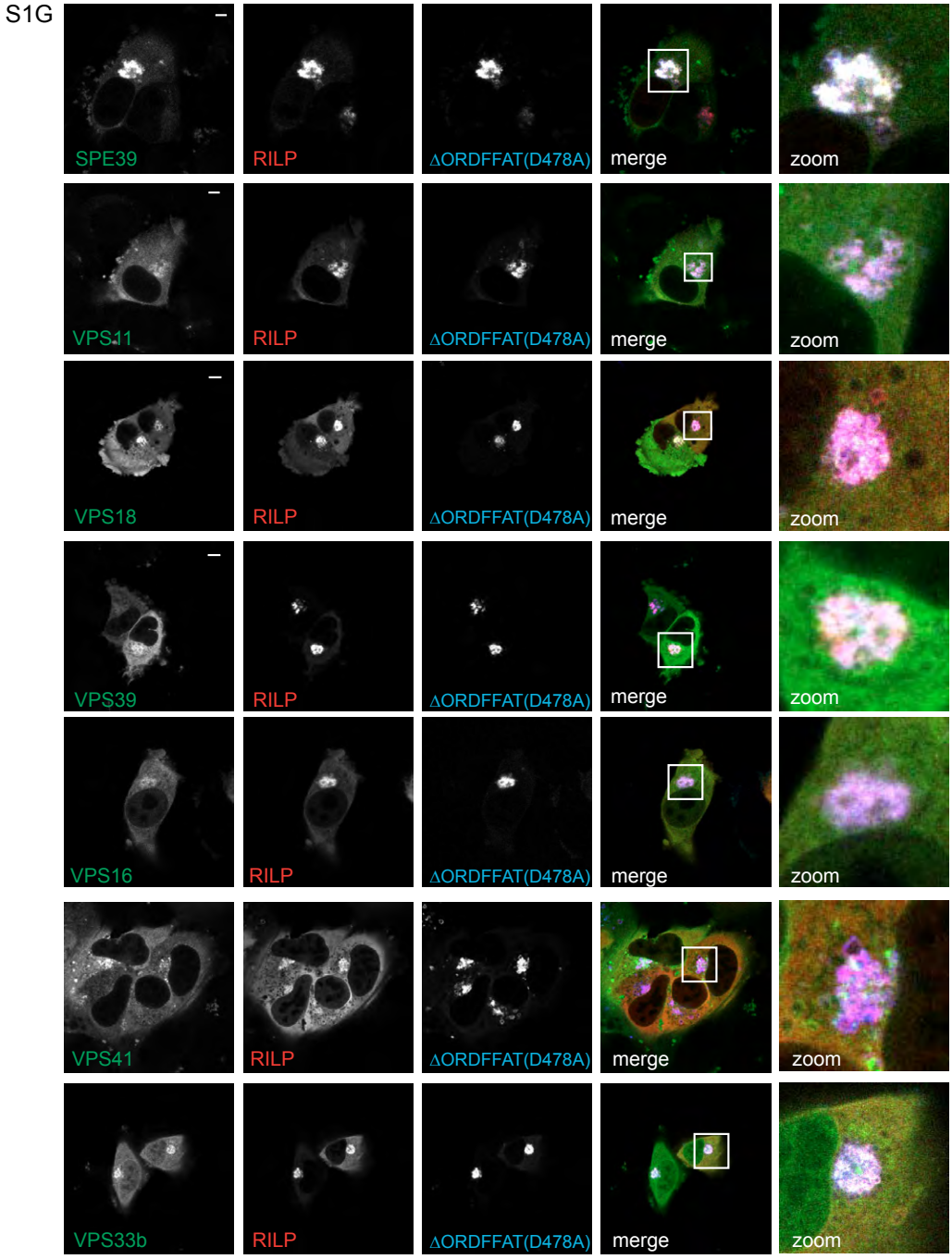

Fig. S1. RILP recruits VPS11, VPS41, VPS39, VPS16, VPS33b and SPE-39 to late endosomes. (**A**) Localization and membrane recruitment of HOPS complex subunits. MelJuSo cells expressing the GFP constructs indicated in combination with myc-RAB7Q67L or HA-RILP (as indicated) were fixed, immunolabelled with myc- or HA-antibodies and imaged by confocal fluorescence microscopy. Zoom-in indicated. Scale bar: 10µm. n>100 (**B)** Localization and endosomal membrane recruitment of VPS33a. MelJuSo cells expressing mRFP-VPS33a in the presence or absence of HA-RILP, GFP-VPS16 or combinations (as indicated) were fixed, immunolabelled with myc- or HA-antibodies and imaged by confocal fluorescence microscopy. Box indicate zoom-in area. Scale bar: 10µm. n>100. (**C**) Relative expression levels of GFP-tagged VPS proteins compared to their endogenous levels. MelJuSo cells were transfected with the constructs indicated and proteins were separated by SDS-PAGE and WB with antibodies indicated. Dark arrow shows position of GFP-tagged constructs, gray arrow the position of endogenous protein. Position of marker proteins indicated. (**D**) Tagged VPS proteins are incorporated into high molecular weight complexes. Lysates of MelJuSo cells expressing GFP-tagged VPS16, VPS11, VPS33b, VPS33a or SPE-39 were size separated by gel filtration. The elution of control proteins (and their mass) is indicated. Fractions of different sizes were separated by SDS-PAGE and WB and probed with antibodies indicated to detect complexes containing the GFP-tagged overexpressed proteins and their endogenous counterparts. For GFP-VPS33a only a very small fraction of total overexpressed protein was incorporated into higher molecular weight complexes, while other GFP tagged-HOPS subunits migrated similar as their untagged endogenous counterparts. MelJuSo cells expressing individual tagged-HOPS subunits (SPE39, VPS11, VPS18, VPS39, VPS41, VPS16, VPS33b) and HA-RILP were co-transfected with (**E**) mRFP-ORP1L (**F**) mRFP-ORP1LΔORD (**G**) mRFP-ORP1LΔORDFFAT(D478A). Cells were fixed and immunolabeled with HA-antibodies before imaging by confocal fluorescence microscopy. Boxed area shows the zoom-in. Scale bar: 10µm. Representative images for n>100.

S2 A

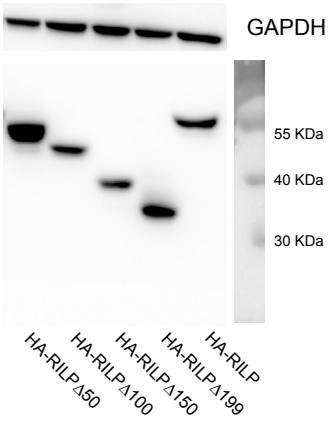
GAPDH
55 KDa
40 KDa
30 KDa
HA-RILP Δ50
HA-RILP Δ100
HA-RILP Δ150
HA-RILP Δ199
HA-RILP

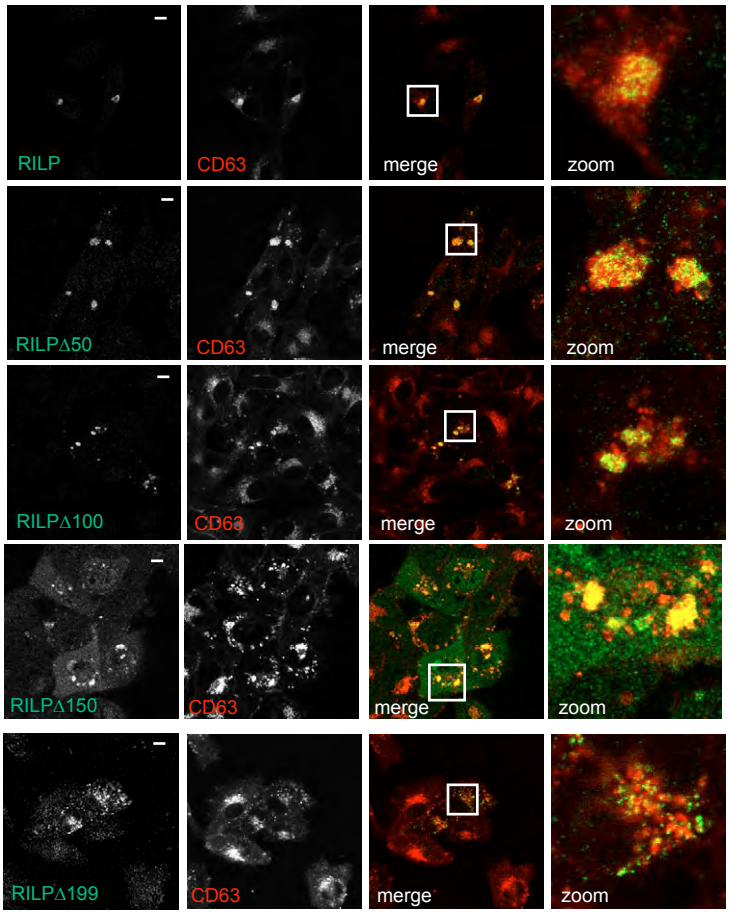
RILP
CD63
merge
zoom
RILPΔ50
CD63
merge
zoom
RILPΔ100
CD63
merge
zoom
RILPΔ150
CD63
merge
zoom
RILPΔ199
CD63
merge
zoom

S2 B

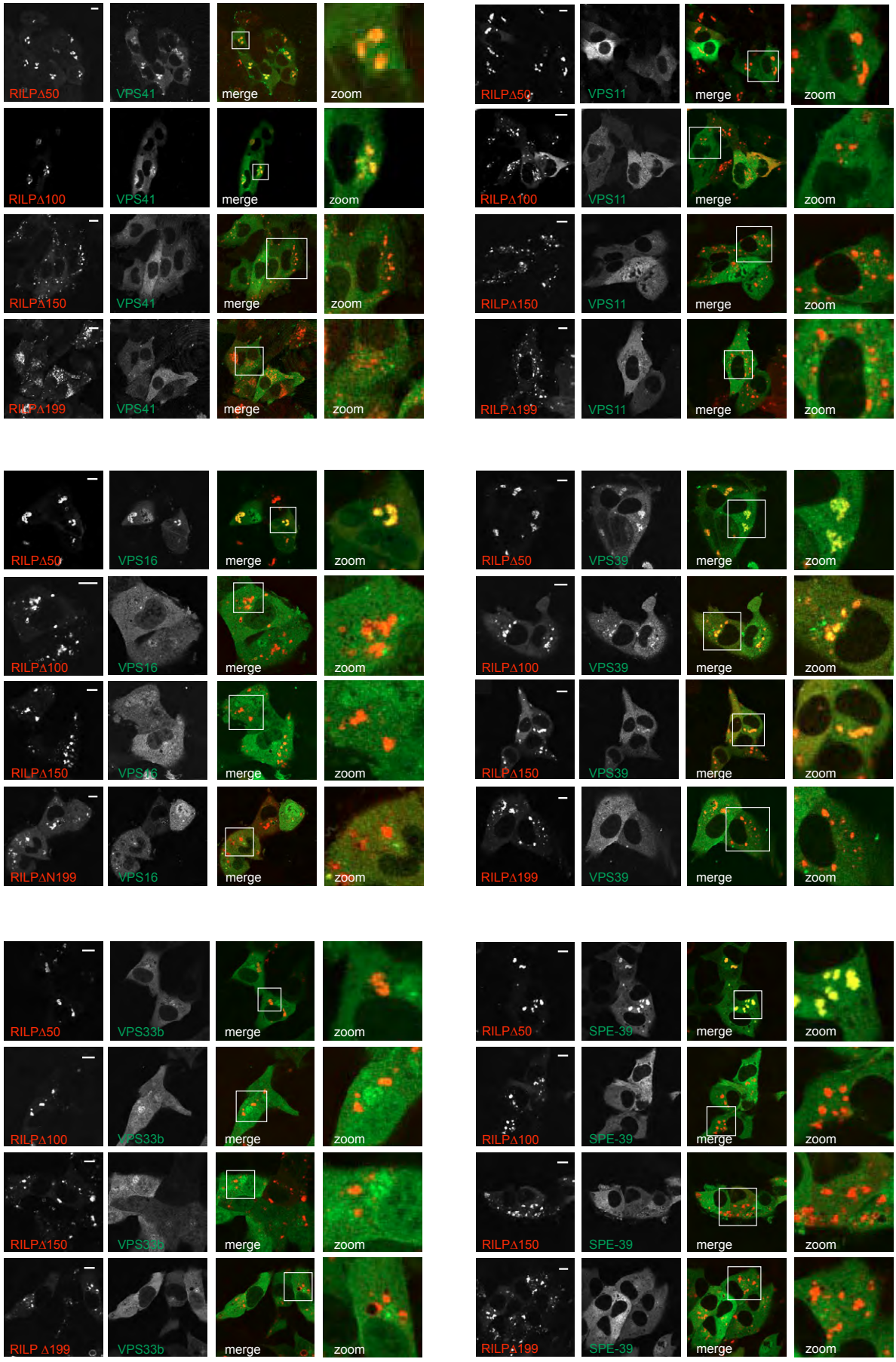
RILPΔ50
VPS41
merge
zoom
RILPΔ100
VPS41
merge
zoom
RILPΔ150
VPS41
merge
zoom
RILPΔ199
VPS41
merge
zoom
RILPΔ50
VPS11
merge
zoom
RILPΔ100
VPS11
merge
zoom
RILPΔ150
VPS11
merge
zoom
RILPΔ199
VPS11
merge
zoom
RILPΔ50
VPS16
merge
zoom
RILPΔ100
VPS16
merge
zoom
RILPΔ150
VPS16
merge
zoom
RILPΔN199
VPS16
merge
zoom
RILPΔ50
VPS39
merge
zoom
RILPΔ100
VPS39
merge
zoom
RILPΔ150
VPS39
merge
zoom
RILPΔ199
VPS39
merge
zoom
RILPΔ50
VPS33b
merge
zoom
RILPΔ100
VPS33b
merge
zoom
RILPΔ150
VPS33b
merge
zoom
RILP Δ199
VPS33b
merge
zoom
RILPΔ50
SPE-39
merge
zoom
RILPΔ100
SPE-39
merge
zoom
RILPΔ150
SPE-39
merge
zoom
RILPΔ199
SPE-39
merge
zoom

S2 C

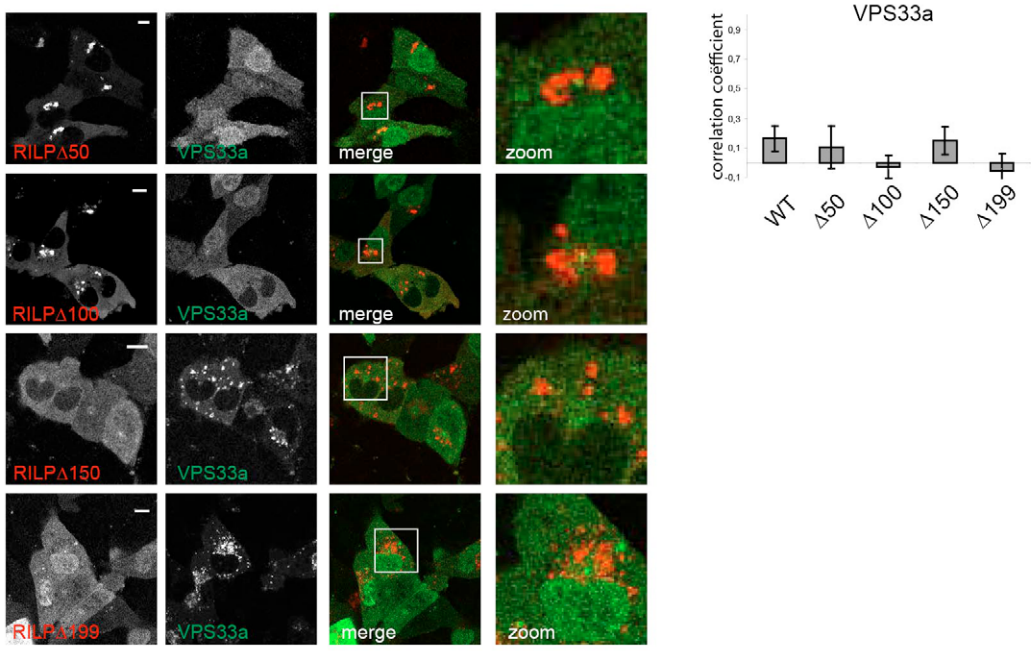

S2 D

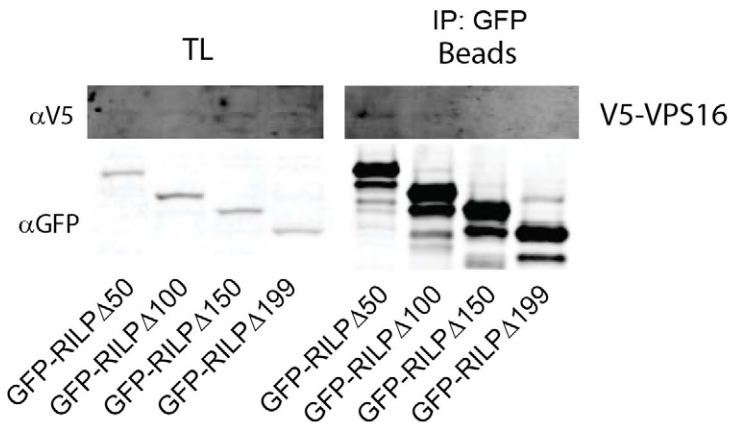

Fig. S2. Binding of HOPS complex subunits to RILP. (**A**) Expression and localization of RILP truncation mutants. Left panel: HA-tagged RILP truncation mutants were expressed in MelJuSo cells. Lysates were separated by SDS-PAGE and WB and detected by anti-HA antibody. Expression of GAPDH is shown as a loading control. Marker proteins indicated. Right panel: MelJuSo cells expressing HA-tagged RILP truncation mutants were fixed, immuno-labeled with anti-HA and anti-CD63 antibodies and imaged by confocal microscopy. Box shows the zoomed-in area. Scale bar: 10µm. n>100 (**B**) Recruitment of VPS11, VPS39, VPS16, VPS33b and SPE-39 to N-terminal truncation mutants of RILP. MelJuSo cells expressing GFP-labelled HOPS subunits as indicated and HA-tagged truncation mutants of RILP (Δ50, Δ100, Δ150 and Δ199 respectively) were fixed, immunolabelled with HA-antibodies and imaged by confocal fluorescence microscopy. Box shows zoomed-in area. Scale bar: 10µm. n>100. **(C)** MelJuSo cells expressing GFP-VPS33a and HA-tagged truncation mutants of RILP (Δ50, Δ100, Δ150 and Δ199 respectively) were fixed, immunolabelled with HA-antibodies and imaged by confocal fluorescence microscopy. Box shows zoomed-in area. Scale bar: 10µm. n>100. Right panel: Quantification of VPS33a recruited to RILP mutants. Mean correlation coefficients + sem are shown. n >10 for each condition. **(D)** Interaction of RILP truncation mutants with V5-VPS16**.** Lysates of Meljuso expressing V5-tagged VPS16 and GFP-RILP truncation mutants were immunoprecipitated (IP) with anti-GFP, then probed by anti-V5 and anti-GFP. TL: total lysate; IP: immunoprecipation.

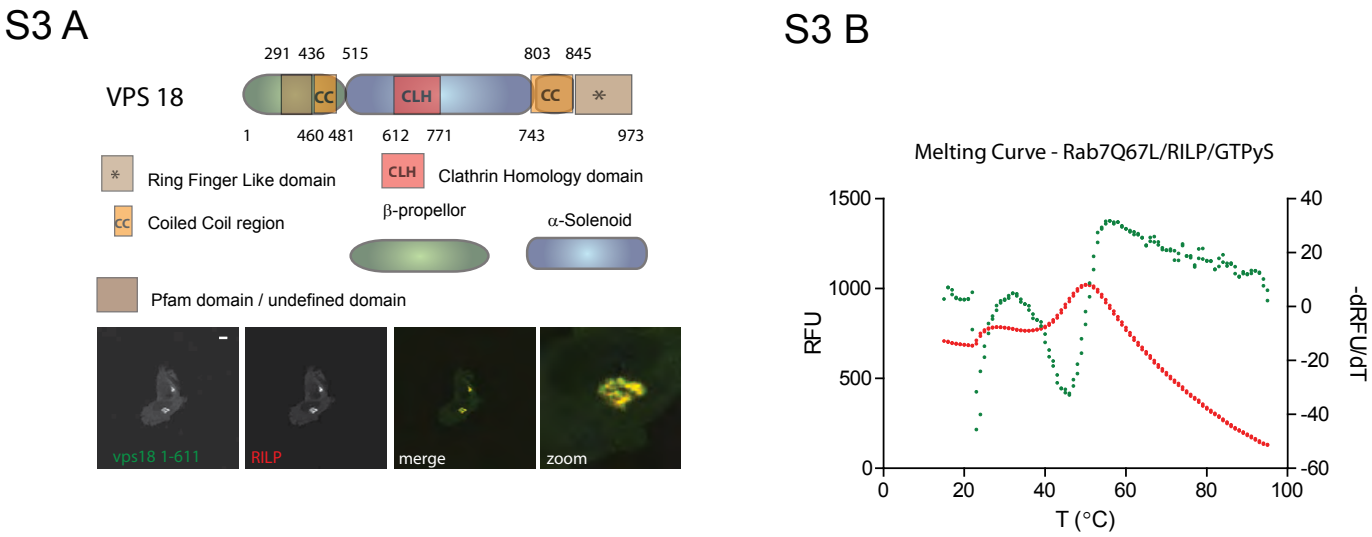

Fig. S3. Proteins used in SPR-experiments. (**A**) The N-terminus of VPS18 is sufficient for RILP recruitment. Upper panel: schematical map of VPS18 domains. Lower panel: MelJuSo cells expressing GFP-VPS18 [1-611] and RILP-HA were fixed, stained with anti-HA antibodies and imaged by confocal microscopy. The N-terminus of VPS18, as used for SPR experiments is recruited to RILP positive endosomes. Bar: 10 µm (**B**) The Rab7Q67L/RILP complex is a stable complex. A Rab7Q67L complex with RILP was generated in the presence of GTP-γS and the temperature stability of the complex was measured. Red line is the melting curve in relative fluorescence units (RFU). The green line is first derivative of melting curve that shows Tm of 55°C (peak).

S4 A

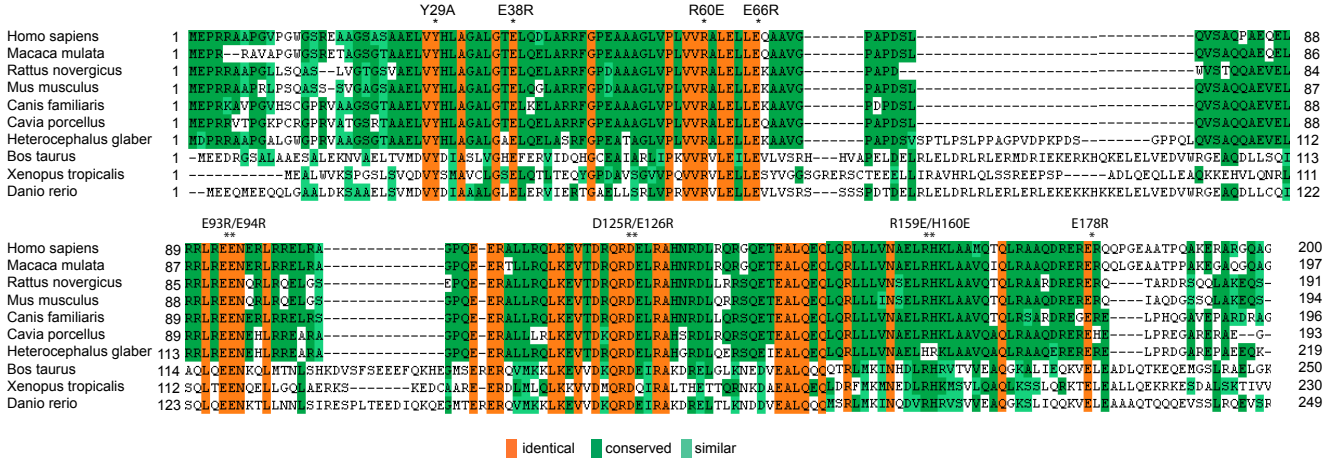

S4 B

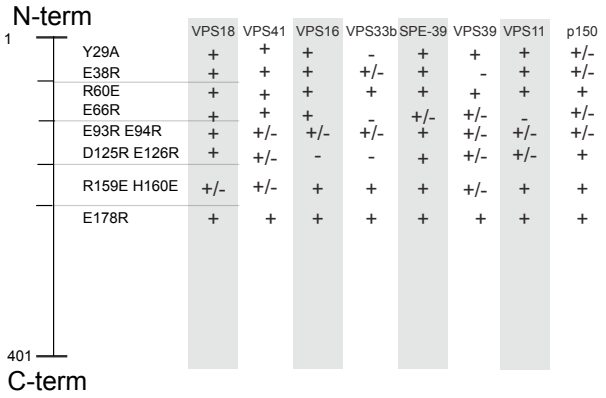

S4 C

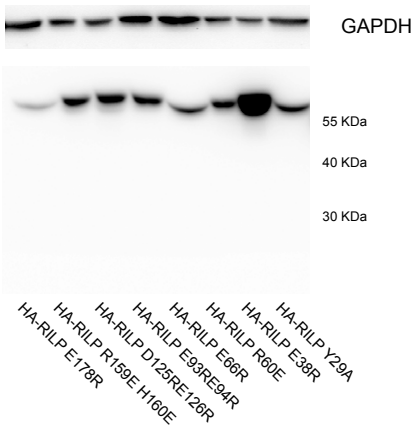

S4 D

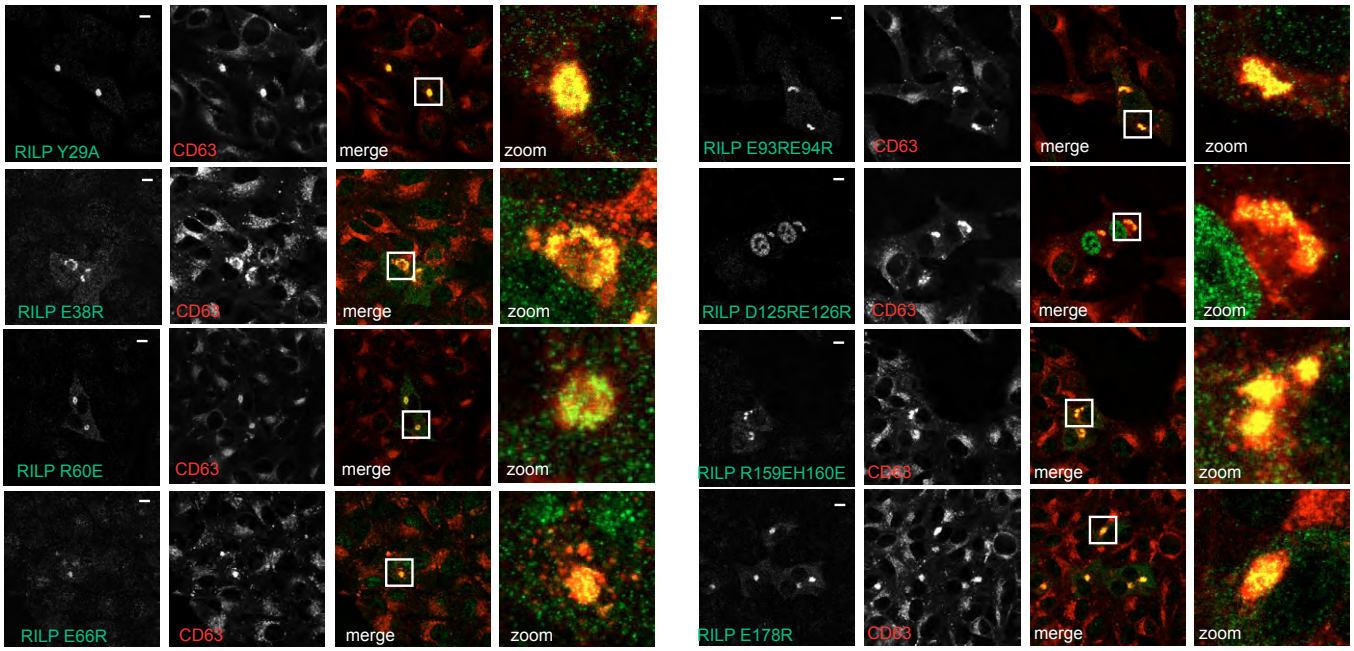

S4 E

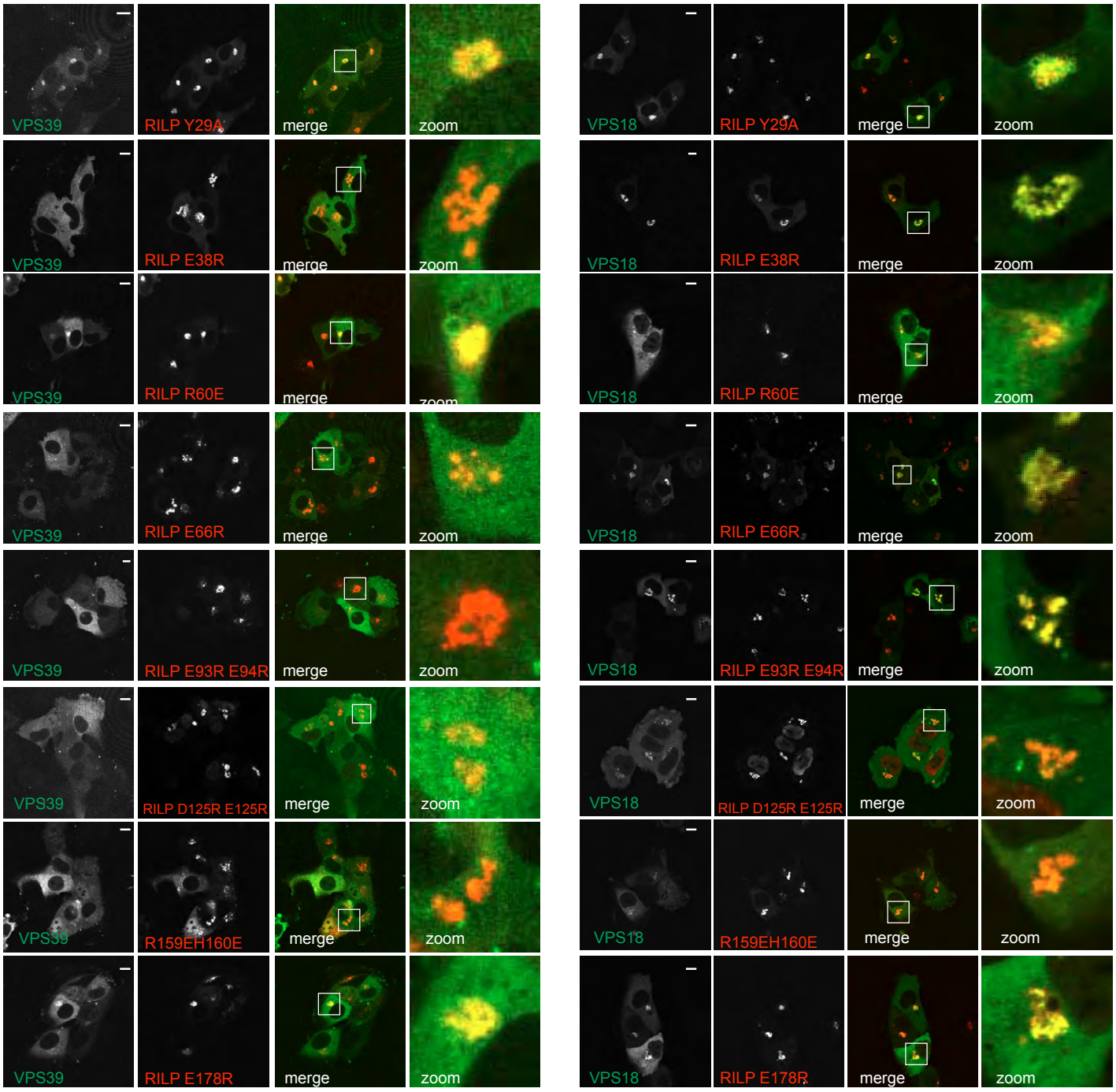
VPS39
RILP Y29A
merge
zoom
VPS18
RILP Y29A
merge
zoom
VPS39
RILP E38R
merge
zoom
VPS18
RILP E38R
merge
zoom
VPS39
RILP R60E
merge
zoom
VPS18
RILP R60E
merge
zoom
VPS39
RILP E66R
merge
zoom
VPS18
RILP E66R
merge
zoom
VPS39
RILP E93R E94R
merge
zoom
VPS18
RILP E93R E94R
merge
zoom
VPS39
RILP D125R E125R
merge
zoom
VPS18
RILP D125R E125R
merge
zoom
VPS39
R159EH160E
merge
zoom
VPS18
R159EH160E
merge
zoom
VPS39
RILP E178R
merge
zoom
VPS18
RILP E178R
merge
zoom

S4 F

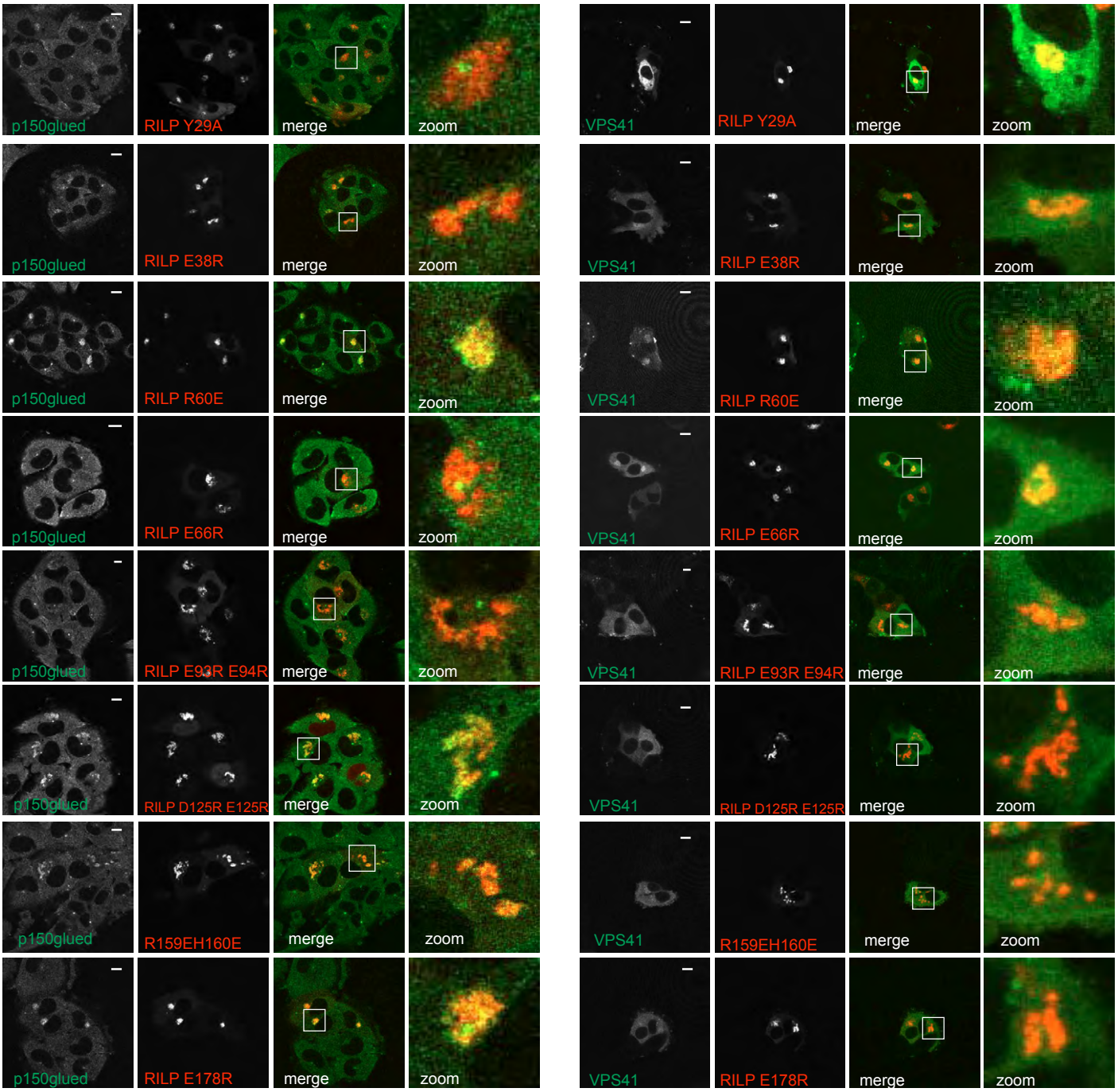
p150glued
RILP Y29A
merge
zoom
VPS41
RILP Y29A
merge
zoom
p150glued
RILP E38R
merge
zoom
VPS41
RILP E38R
merge
zoom
p150glued
RILP R60E
merge
zoom
VPS41
RILP R60E
merge
zoom
p150glued
RILP E66R
merge
zoom
VPS41
RILP E66R
merge
zoom
p150glued
RILP E93R E94R
merge
zoom
VPS41
RILP E93R E94R
merge
zoom
p150glued
RILP D125R E125R
merge
zoom
VPS41
RILP D125R E125R
merge
zoom
p150glued
R159EH160E
merge
zoom
VPS41
R159EH160E
merge
zoom
p150glued
RILP E178R
merge
zoom
VPS41
RILP E178R
merge
zoom

S4 G

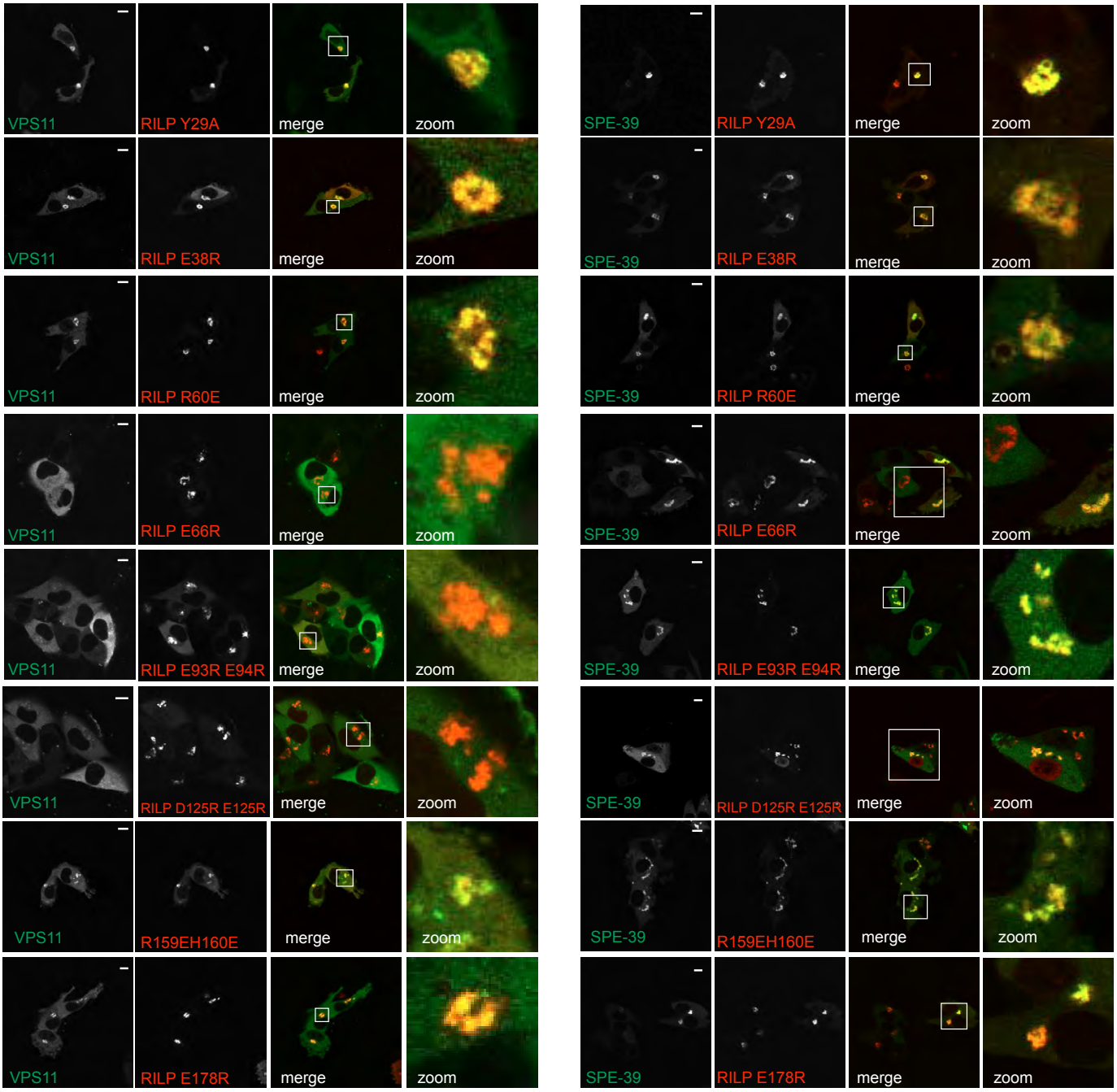
VPS11
RILP Y29A
merge
zoom
SPE-39
RILP Y29A
merge
zoom
VPS11
RILP E38R
merge
zoom
SPE-39
RILP E38R
merge
zoom
VPS11
RILP R60E
merge
zoom
SPE-39
RILP R60E
merge
zoom
VPS11
RILP E66R
merge
zoom
SPE-39
RILP E66R
merge
zoom
VPS11
RILP E93R E94R
merge
zoom
SPE-39
RILP E93R E94R
merge
zoom
VPS11
RILP D125R E125R
merge
zoom
SPE-39
RILP D125R E125R
merge
zoom
VPS11
R159EH160E
merge
zoom
SPE-39
R159EH160E
merge
zoom
VPS11
RILP E178R
merge
zoom
SPE-39
RILP E178R
merge
zoom

S4 H

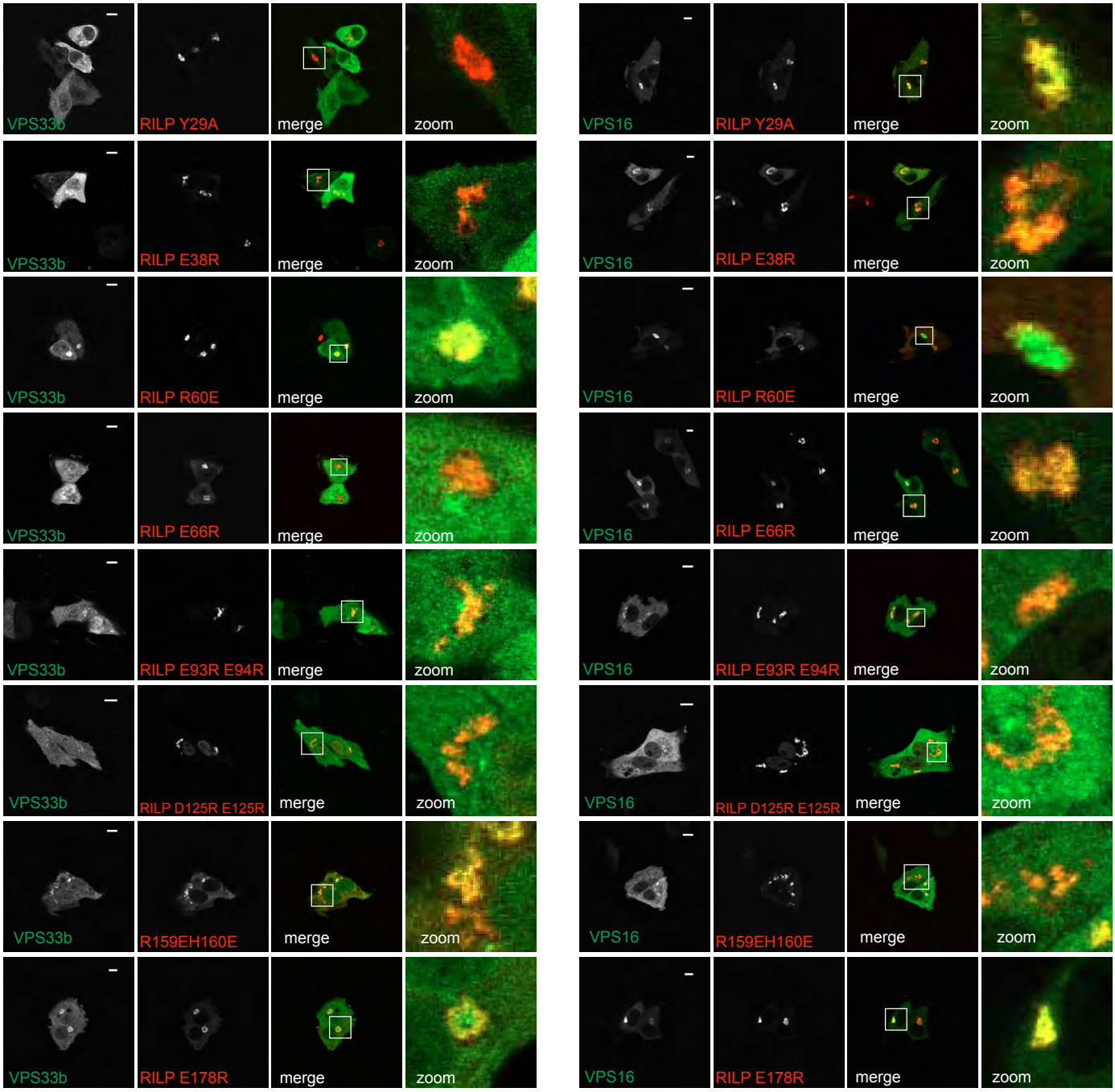
VPS33b
RILP Y29A
merge
zoom
VPS16
RILP Y29A
merge
zoom
VPS33b
RILP E38R
merge
zoom
VPS16
RILP E38R
merge
zoom
VPS33b
RILP R60E
merge
zoom
VPS16
RILP R60E
merge
zoom
VPS33b
RILP E66R
merge
zoom
VPS16
RILP E66R
merge
zoom
VPS33b
RILP E93R E94R
merge
zoom
VPS16
RILP E93R E94R
merge
zoom
VPS33b
RILP D125R E125R
merge
zoom
VPS16
RILP D125R E125R
merge
zoom
VPS33b
R159EH160E
merge
zoom
VPS16
R159EH160E
merge
zoom
VPS33b
RILP E178R
merge
zoom
VPS16
RILP E178R
merge
zoom

S4I

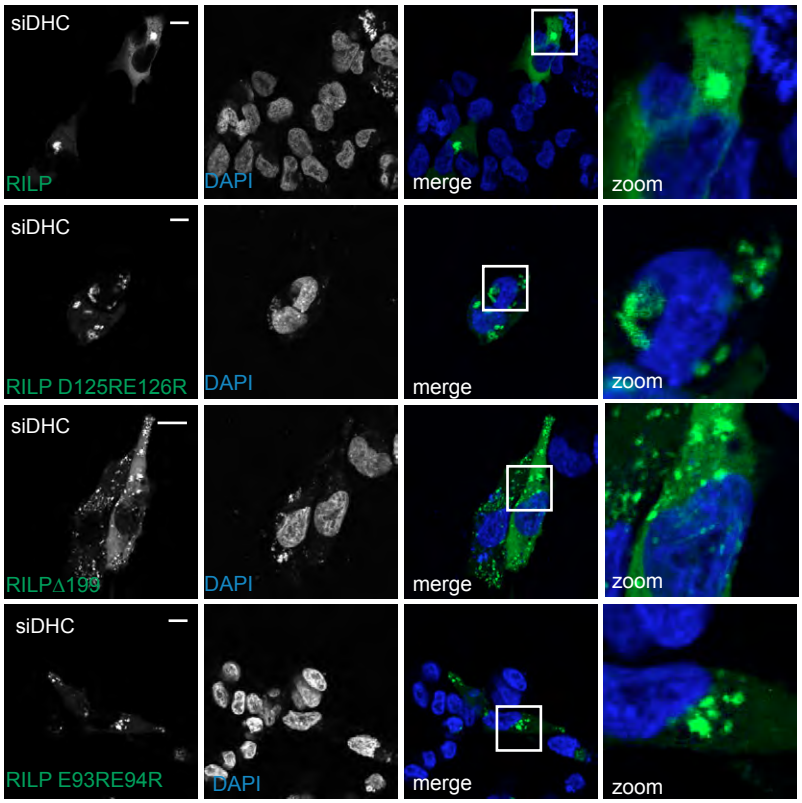
siDHC
RILP
DAPI
merge
zoom
siDHC
RILP D125RE126R
DAPI
merge
zoom
siDHC
RILPΔ199
DAPI
merge
zoom
siDHC
RILP E93RE94R
DAPI
merge
zoom

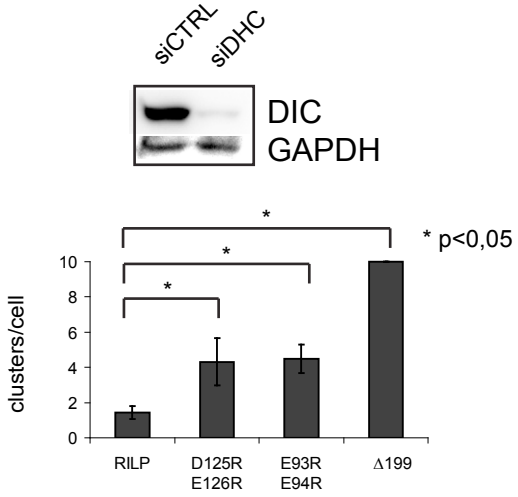
siCTRL
siDHC
DIC
GAPDH
clusters/cell
10
8
6
4
2
0
*
*
*
* p<0,05
RILP
D125R
E126R
E93R
E94R
Δ199

S4 J

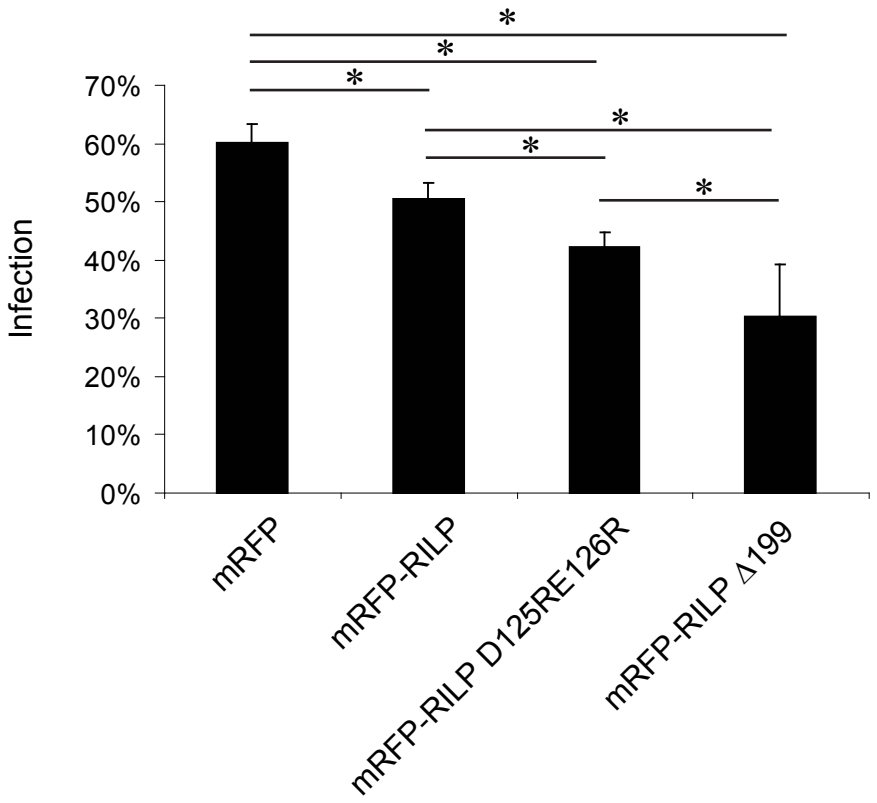

Fig. S4. RILP point mutants and the binding of HOPS subunits. Sequence alignment of the RILP N-terminus (*Homo sapiens* AA 1-200) and nine other species. Red: identical amino acids, dark green: conserved amino-acids, light green: similar amino acids. Asterisks indicate charged amino acids mutated in the opposite charge in our study. (**B**) Semi-quantitative representation of $p150^{Glued}$ and HOPS subunit recruitment to RILP mutants (see Fig 4A, S4E-H). Levels of recruitment are depicted as '+' (strong recruitment) to '–' (no recruitment). (**C**) Expression levels of RILP point mutants expressed in MelJuSo cells. Cell lysates were separated by SDS-PAGE and WB probed with an anti-HA antibody. GAPDH is shown as a loading control. Marker proteins indicated. (**D**) MelJuSo cells expressing HA-tagged RILP point mutants were fixed, immuno-labeled with anti-HA and anti-CD63 antibodies and imaged by confocal microscopy. Boxed area zoomed-in. Scale bar: 10µm. Shown is representative cell of n>100. (**E**) RILP mutants and VPS39 and VPS18. MelJuSo cells expressing HA-RILP mutants (as indicated) and MYC-mRFP-VPS39 (left) or GFP-VPS18 (right) were fixed and immunolabeled with HA-antibodies and imaged by confocal fluorescence microscopy. Scale bar: 10µm. Representative of n>100 (**F**) RILP mutants and $p150^{Glued}$ and VPS41. MelJuSo cells expressing GFP-RILP mutants (as indicated) were fixed and immunolabelled with $p150^{Glued}$-antibodies (left). MelJuSo cells expressing HA-RILP mutants and GFP-VPS41 were fixed and immunolabeled with HA-antibodies and imaged by confocal fluorescence microscopy (right). Scale bar: 10µm. n>100 (**G**) RILP mutants, VPS11 and SPE-39. MelJuSo cells expressing HA-RILP mutants and GFP-VPS11 (left) or SPE-39-GFP (right) were fixed, immunolabeled with HA-antibodies and imaged by confocal fluorescence microscopy. Scale bar: 10µm. n>100 (**H**) RILP mutants, VPS33b and VPS16. MelJuSo cells expressing HA-RILP mutants and GFP-VPS33b (left) or GFP-VPS16 (right) were fixed, immunolabeled with HA-antibodies and imaged by confocal fluorescence microscopy. Scale bar: 10µm. n>100. (**I**) MelJuSo cells silenced for Dynein heavy chain and expressing HA-RILP, HA-RILPΔ199, HA-RILP D125RE126R or HA-RILP E93RE94R were fixed, immunolabelled with HA-antibodies and DAPI and imaged by CLSM. Scale bar: 10µm, representative of n>100. Right bottom panel: Quantification shows average number of individual vesicle clusters and/or free vesicles per cell. Cells with >10 clusters were set at 10 (means + SD; n>100). Right top panel: Western blot shows silencing for Dynein heavy chain by staining for co-depleted Dynein intermediate chain (Raaijmakers et al., 2012). (**J**) HAP-1 cells expressing mRFP, mRFP-RILP, mRFP-RILPD125RE126R or mRFP-RILPΔ199 were infected with rVSV-GP-EboV for 8 hours. After successful infection, the virus produces GFP in the host cell's cytosol which is detected and quantified by flow cytometry. Shown is the percentage virus infection (by GFP) in mRFP-RILP or mRFP-RILP mutant expressing cells (mean + sem). * $p<0,05$.

	fwd	
primerset 1	CCCAAAGCTTGCCACCATGGGTAAGCCTATCCCTAACCCT CTCCTCGGTCTCGATTCTACGATGGACTGCTACACGGCGA	vps16
primerset 2	CCCAGAATTCCATGGCTTTTCCCCATCG	vps33b
primerset 3	CCCAGGATCCATGGCGGAAGCAGAGGAGCA	vps41
primerset 4	ATGGCGGCCTACCTGCAGTG	vps11
primerset 5	CCCAGAATTCACCACCATGAATCGGACAAAGGGTGA	spe39
primerset 6	CCCAGGATCCATGAATCGGACAAAGGGTGA	spe39
primerset 7	agaggAGGcgccagcagcctggcgaag	RILP E178R
primerset 8	gctgGAGGAGaagctggcggccatgcagac	RILP R159EH160E
primerset 9	gcggCGCCGActccgggcgcacaaccgc	RILP D125RE126R
primerset 10	gcggAGGAGGaacgagcgcctccgcagg	RILP E93RE94R
primerset 11	tcttgAGAcaggctgccgtggggccc	RILP E66R
primerset 12	tggtgGAGgcgctggagctcttggaaca	RILP R60E
primerset 13	agcgcCTCcaccactagcggcaccagc	RILP E38R
primerset 14	cttgtgGCCcatctagccggggccctgg	RILP Y26A
	rev	
primerset 1	cccagaattcTCACTTCTTCTGGGCTTGTG	vps16
primerset 2	CCCAGAATTCTCAGGCTTTCACCTCACTCA	vps33b
primerset 3	CCCAGGATCCCTATTTTTTCATCTCCAA	vps41
primerset 4	CCCAGAATTCTTAAGTGCCCC-TCCTGGAGT	vps11
primerset 5	CCCAGGATCCAAATTCTTCCATCGAATTTGC	spe39
primerset 6	CCCAGAATTCTCAAGCGTAATCAGGAACGT	spe39
primerset 7	tggcgCCTcctctcgcggtcctgcgc	RILP E178R
primerset 8	ggagTCGGCGccgctgtcggtccgtgacc	RILP R159EH160E
primerset 9	ggagTCGGCGccgctgtcggtccgtgacc	RILP D125RE126R
primerset 10	cgttCCTCCTccgcagccgccgcagctcc	RILP E93RE94R
primerset 11	gcctgTCTcaagagctccagcgcccgc	RILP E66R
primerset 12	agcgcCTCcaccactagcggcaccagc	RILP R60E
primerset 13	tgcagCCTagtgcccagggccccggc	RILP E38R
primerset 14	tagatgGGCcacaagctccgcggccgat	RILP Y26A

Table S1. Primers used in the study.